Soil Dynamics and Earthquake Engineering, 115(2018), 634-651.
https://doi.org/10.1016/j.soildyn.2018.08.027

Influence of earthquake duration on the response of steel moment frames

Miguel A. Bravo-Haro & Ahmed Y. Elghazouli[1]

Department of Civil and Environmental Engineering, Imperial College London, UK
miguel.bravo-haro14@imperial.ac.uk, a.elghazouli@imperial.ac.uk

ABSTRACT

The influence of ground motion duration on the seismic response of steel moment frames is examined is this paper, with due consideration for cyclic degradation effects. A set of 77 spectrally equivalent pairs of short and long records is utilised in detailed nonlinear dynamic assessments in order to isolate the effects of ground motion duration. The influence of duration is firstly evaluated considering degrading and non-degrading idealised bilinear SDOF systems, for various levels of lateral strength representing practical ranges encountered in design. Subsequently, a sensitivity assessment focusing on the main parameters affecting the response of hysteretic degrading models is carried out through comparative incremental dynamic analysis. Whilst the effect of duration becomes more pronounced with the increase in lateral strength demands, particularly when approaching collapse, the cyclic degradation rate is shown to play a significant role even at lower levels typically associated with design. The performance of EC8-compliant frames indicates a higher probability of collapse when long-duration ground motion records are used, with a typical reduction of about 20% in the collapse capacity, in comparison with short-duration cases. The influence of duration is also examined through collapse capacity spectra, based on the seismic performance of 50 steel moment frames, which show that considerable reduction in the structural collapse capacity of structural systems occurs when relatively long duration records are adopted, for a wide range of dynamic characteristics. This becomes particularly evident in the case of buildings with relatively significant cyclic deterioration rates, where collapse capacity reductions up to 40% due to the influence of earthquake duration are obtained.

Keywords: steel moment frames; ground motion duration; cyclic degradation; spectrally equivalent records.

1. INTRODUCTION

Over the past two decades, several studies have examined the influence of earthquake duration on seismic response, and the significant role of longer earthquakes in liquefaction proneness is particularly well documented (e.g., **Verdugo and González 2015**; **Bhattacharya et al. 2011**). In the case of structural seismic demand, the findings have depended on the parameters considered. On the one hand, studies considering only peak deformations or peak inter-storey drifts did not report clear correlations with duration (e.g., **Cornell 1997**; **Iervolino et al. 2006**). On the other hand, studies considering cumulative response indices, such as energy dissipation or number of inelastic cycles, showed an influence of duration on global response measures (e.g., **Bommer et al. 2004**; **Dutta and Mander 2001**; **Hancock and Bommer 2006**). Overall, however, seismic codes typically do not account explicitly for the duration of ground motion.

Due to the increasing availability of reliable long ground motion records data from large magnitude earthquakes, mostly from subduction zones such as Chile and Japan, the study of earthquake duration effects has become more robust. For instance, in the past, because of the scarcity of records, long duration ground motions were artificially created (e.g., **Sarieddine and Lin 2013**; **Tremblay 1998**; **Xie and Zhang 1988**; **Saragoni and Hart 1973**). Likewise, in order to isolate the effect of duration from inherent characteristics such as frequency content or amplitude, the spectral content of ground motion records can be altered in order to obtain equivalent response spectra (e.g., **Ou et al. 2013**; **Hancock and Bommer 2007**). A procedure, introduced first by **Foschaar et al. (2012)** and later refined by **Chandramohan et al. (2016)** can be followed, where pairs of spectrally equivalent short and long ground motion records can be used such that the spectral content is largely the same.

[1] Corresponding author

More recent studies on collapse capacity assessments included a resurgence of interest on duration effects (e.g., **Raghunandan and Liel 2013**; **Chandramohan et al. 2016**; **Barbosa et al. 2017**). Reductions of 29% in median collapse capacity due to earthquake duration in a single steel moment frame were reported by **Chandramohan et al. (2016)**, while **Raghunandan and Liel (2013)** found reductions in the range of 26%-56% using a set of 17 RC buildings. Similar observations were also made by **Barbosa et al. (2017)**, showing that longer duration motion tends to have a notable effect on collapse level assessments. In contrast, there are disagreements in these studies on the effect of cyclic deterioration when the influence of duration is considered, with some studies reporting an insignificant effect (**Raghunandan and Liel 2013**), whilst others indicating its relative importance (**Chandramohan et al. 2016**). However, the latter two studies are not directly comparable since they used different procedures to account for earthquake duration effects.

The influence of long duration on the seismic response of steel moment frames, designed to the provisions of Eurocode 3 (**CEN 2005**) and Eurocode 8 (**CEN 2004a**), is evaluated in this paper. The study comprises a family of 50 multi-storey buildings, representative of typical low-to-medium-rise construction in Europe, with a wide range of structural characteristics. The structural collapse capacity is also computed through Incremental dynamic analysis (IDA) (**Vamvatsikos and Cornell 2002**), by using detailed structural models for four selected cases with different heights, and equivalent idealised single-degree-of-freedom (ESDOF) models incorporating P-Delta effects for the other cases. A set of 77 spectrally equivalent pairs of short and long records is collated and utilised. For this purpose, shallow crustal events are used for the short duration, and recent large magnitude subduction zone events are considered for the long duration. The influence of duration is initially assessed considering degrading and non-degrading (i.e. in-cycle and cyclic deterioration of strength and stiffness in structural components) bilinear hysteretic models in order to establish a basis for comparison. Subsequently, a sensitivity analysis of the main parameters affecting the response of a hysteretic degrading model is undertaken through comparative IDA. Particular attention is given to the cyclic degradation rate, for which a more detailed assessment is carried out. The influence of duration is also examined through the use of collapse capacity spectra (**Adam and Jäger 2012**), where the collapse capacity is determined with respect to the fundamental period of vibration. Finally, the influence of the global lateral structural stiffness, as well as the cyclic deterioration rate, on earthquake duration effects is considered, and the main findings are discussed.

2. GROUND MOTION AND STRUCTURAL SYSTEMS

2.1. Earthquake records

Several approaches have been suggested previously for quantifying ground motion duration. **Bommer and Martinez-Pereira (1999)** referred to 30 different metrics to define duration. Out of these, the significant duration ($D_{s_{5-75}}$) proposed by **Trifunac and Brady (1975)** is used herein to characterise the ground motion records, as several studies indicated its suitability for assessing the performance of structural systems (**Barbosa et al. 2017; Chandramohan et al. 2016; Foschaar et al. 2012**). Two paired sets of spectrally equivalent short and long records are selected. Large magnitude earthquakes in subduction zones were chosen for the long duration motion (e.g., Maule earthquake, Chile 2010; and Tohoku earthquake, Japan 2011). As those records were collected from different databases, they were filtered and baseline-corrected (**Boore and Bommer 2005**). Similarly, ground motions due to shallow crustal earthquakes were selected from the PEER NGA-West 2 database (**Ancheta et al. 2014**). Subsequently, a matching process was performed in order to minimise the mean squared error of the 5%-damped linear response spectra between short and long records. To enable this procedure, response spectra of short ground motion records were scaled where necessary by a factor limited to 5. This process ruled out records with very low spectral intensity, which would need larger scaling factors to match its long duration response spectrum counterpart. The criteria to establish a ground motion as long or short duration were based on a significant duration, $D_{s_{5-75}}$, higher than 25 s for long duration and lower than 25 s for short duration. Overall, 77 pairs of records were selected (i.e., 144 individual ground motions). The list of earthquakes, and number of ground motions considered for both sets, is given in Table 1. Figure 1 (a) and (b) also show the 77 individual response spectra for short and long duration records, respectively, and Figure 1 (c) shows a direct comparison of their median spectra.

Table 1. Long duration ground motions and their spectrally equivalent short duration records

Long duration records				Short duration records				
Earthquake	Magnitude	Station name	Ds_{5-75}	Earthquake	Magnitude	Station name	Scale factor	Ds_{5-75}
1999 Kocaeli, Turkey	7.51	Bursa Tofas	26	1999 Chi-Chi, Taiwan-04	6.20	KAU085	4.41	20
1999 Kocaeli, Turkey	7.51	Bursa Tofas	22	1992 Landers	7.28	Yermo Fire Station	0.54	7
1999 Kocaeli, Turkey	7.51	Fatih	10	1999 Chi-Chi, Taiwan-06	6.30	HWA025	5.00	3
1999 Kocaeli, Turkey	7.51	Fatih	28	1999 Chi-Chi, Taiwan-02	5.90	HWA059	4.74	8
1992 Landers	7.28	Indio - Jackson Road	22	1992 Cape Mendocino	7.01	Petrolia	0.47	3
1992 Landers	7.28	Indio - Jackson Road	26	1994 Northridge-01	6.69	Camarillo	1.04	14
1992 Landers	7.28	Thousand Palms Post Office	26	1999 Chi-Chi, Taiwan-06	6.30	CHY024	0.77	10
1992 Landers	7.28	Thousand Palms Post Office	25	1986 Taiwan SMART1(45)	7.30	SMART1 I11	0.75	11
2010 El Mayor-Cucapah	7.20	Chihuahua	24	1999 Hector Mine	7.13	Amboy	1.47	11
2010 El Mayor-Cucapah	7.20	Chihuahua	27	2010 Darfield, New Zealand	7.00	DORC	2.97	16
2010 El Mayor-Cucapah	7.20	Ejido Saltillo	33	1999 Chi-Chi, Taiwan	7.62	TCU075	0.54	18
2010 El Mayor-Cucapah	7.20	Ejido Saltillo	33	1999 Chi-Chi, Taiwan	7.62	TCU101	0.82	16
2010 El Mayor-Cucapah	7.20	Tamaulipas	27	1992 Landers	7.28	Amboy	1.55	17
2010 El Mayor-Cucapah	7.20	Tamaulipas	28	2010 Darfield, New Zealand	7.00	Canterbury Aero Club	1.26	15
1992 Landers	7.28	Indio - Coachella Canal	25	1989 Loma Prieta	6.93	SF - Presidio	0.57	3
1992 Landers	7.28	Indio - Coachella Canal	25	1999 Chi-Chi, Taiwan-06	6.30	CHY100	1.62	12
2011 Tohoku, Japan	9.00	Yanagawa	74	1983 Coalinga-05	5.77	Palmer Ave	2.27	2
2011 Tohoku, Japan	9.00	Yanagawa	71	2004 Niigata, Japan	4.11	NIGH10	4.11	6
2011 Tohoku, Japan	9.00	Fukushima	77	1983 Mammoth Lakes-11	4.14	Convict Creek	4.14	4
2011 Tohoku, Japan	9.00	Fukushima	76	1979 Coyote Lake	5.74	Gilroy Array #3	1.22	2
2011 Tohoku, Japan	9.00	Iitate	76	1983 Coalinga-05	5.77	Coalinga-14th & Elm (Old CHP)	1.16	1
2011 Tohoku, Japan	9.00	Iitate	78	1987 Whittier Narrows-01	5.99	Orange Co. Reservoir	4.03	3
2011 Tohoku, Japan	9.00	Kohriyama	70	2008 Iwate	6.90	Shinchicho Yacigoya	5.00	6
2011 Tohoku, Japan	9.00	Kohriyama	67	1981 Taiwan SMART1(5)	4.76	SMART1 M02	4.76	3
2011 Tohoku, Japan	9.00	Nihommatsu	76	2003 Big Bear City	4.92	Big Bear Solar Observatory	4.00	2
2011 Tohoku, Japan	9.00	Nihommatsu	74	1987 Whittier Narrows-01	5.99	Canyon Country -WLost Cany	4.29	3
2011 Tohoku, Japan	9.00	Inawashiro	80	1992 Erzican, Turkey	6.69	Erzincan	0.73	2
2011 Tohoku, Japan	9.00	Inawashiro	80	1994 Northridge-01	6.69	Jensen Filter Plant Administrative Building	0.67	4
2011 Tohoku, Japan	9.00	Aiduwakamatsu	57	2007 Chuetsu-oki	6.80	Toyotsu Nakano	2.28	2
2011 Tohoku, Japan	9.00	Aiduwakamatsu	69	1984 Morgan Hill	6.19	Anderson Dam (Downstream)	1.55	2
2011 Tohoku, Japan	9.00	Fukushima	77	1999 Chi-Chi, Taiwan-06	6.30	CHY024	1.78	7
2011 Tohoku, Japan	9.00	Fukushima	77	1980 Irpinia, Italy-01	6.90	Auletta	3.19	13
2011 Tohoku, Japan	9.00	Kawamata	81	2000 Yountville	5.00	Napa - Napa College	1.67	2
2011 Tohoku, Japan	9.00	Kawamata	85	1987 Whittier Narrows-01	5.99	El Monte - Fairview Av	1.07	2
2011 Tohoku, Japan	9.00	Miharu	79	1999 Chi-Chi (aftershock 3), Taiwan	6.20	CHY014	4.00	6
2011 Tohoku, Japan	9.00	Miharu	76	1997 Northwest China-01	5.90	Jiashi	2.47	2
2011 Tohoku, Japan	9.00	Miyakoji	68	2004 Parkfield-02, CA	6.19	Parkfield - Cholame 5W	3.03	2
2011 Tohoku, Japan	9.00	Miyakoji	71	2004 Parkfield-02, CA	6.19	Parkfield - Cholame 3E	1.26	1

Table 1 (continued). Long duration ground motions and their spectrally equivalent short duration records

Long duration records				Short duration records				
Earthquake	Magnitude	Station name	Ds_{5-75}	Earthquake	Magnitude	Station name	Scale factor	Ds_{5-75}
2011 Tohoku, Japan	9.00	Naruko	71	1980 Irpinia, Italy-01	6.90	Tricarico	5.00	14
2011 Tohoku, Japan	9.00	Naruko	71	1999 Chi-Chi, Taiwan-06	6.30	TCU118	4.63	24
2011 Tohoku, Japan	9.00	Sakunami	75	1999 Chi-Chi, Taiwan-02	5.90	TCU067	5.00	5
2011 Tohoku, Japan	9.00	Sakunami	67	1991 Sierra Madre	5.61	Altadena - Eaton Canyon	1.26	1
2011 Tohoku, Japan	9.00	Iwanuma	80	1999 Chi-Chi, Taiwan-03	6.20	TCU138	3.62	5
2011 Tohoku, Japan	9.00	Iwanuma	70	1999 Chi-Chi, Taiwan-06	6.30	CHY039	4.65	14
2011 Tohoku, Japan	9.00	Shiroishi	77	1979 Imperial Valley-06	6.53	El Centro Array #4	0.93	3
2011 Tohoku, Japan	9.00	Shiroishi	68	1992 Landers	7.28	Boron Fire Station	3.62	8
2011 Tohoku, Japan	9.00	Kakuda	69	1995 Kobe, Japan	6.90	Takarazuka	0.64	2
2011 Tohoku, Japan	9.00	Kakuda	71	1999 Hector Mine	7.13	Temecula - 6th & Mercedes	4.91	13
2011 Tohoku, Japan	9.00	Iwanuma	70	2009 L'Aquila, Italy	6.30	Celano	3.58	4
2011 Tohoku, Japan	9.00	Iwanuma	66	1999 Chi-Chi, Taiwan-06	6.30	TCU138	3.91	14
2011 Tohoku, Japan	9.00	Shiroishi	70	2007 Chuetsu-oki	6.80	Shiozawa Building, Minamiunuma	2.73	11
2011 Tohoku, Japan	9.00	Shiroishi	70	2007 Chuetsu-oki	6.80	NIG013	2.00	12
2011 Tohoku, Japan	9.00	Higashine	73	1994 Northridge-01	6.69	Castaic - Old Ridge Route	0.38	4
2011 Tohoku, Japan	9.00	Higashine	69	1984 Morgan Hill	6.19	San Justo Dam (L Abut)	2.71	11
2011 Tohoku, Japan	9.00	Kaminoyama	86	1989 Loma Prieta	6.93	Los Gatos - Lexington Dam	0.34	2
2011 Tohoku, Japan	9.00	Kaminoyama	81	2007 Chuetsu-oki	6.80	Joetsu City	0.74	14
2011 Tohoku, Japan	9.00	Yonezawa	78	1999 Chi-Chi, Taiwan-05	6.20	CHY063	4.89	13
2011 Tohoku, Japan	9.00	Yonezawa	75	1994 Northridge-01	6.69	Sylmar - Olive View Med FF	0.44	3
2011 Tohoku, Japan	9.00	Tendou	71	1976 Friuli (aftershock 13), Italy	6.00	San Rocco	1.65	3
2011 Tohoku, Japan	9.00	Yamagata	79	2010 Darfield, New Zealand	7.00	Shirley Library	0.88	12
2011 Tohoku, Japan	9.00	Yamagata	85	1999 Chi-Chi, Taiwan-03	6.20	CHY088	3.34	12
2011 Tohoku, Japan	9.00	Takahata	82	1999 Chi-Chi, Taiwan	7.62	ILA062	2.53	14
2011 Tohoku, Japan	9.00	Takahata	80	1979 Coyote Lake	5.74	Gilroy Array #4	0.83	5
2011 Tohoku, Japan	9.00	Yonezawa	65	2007 Chuetsu-oki	6.80	NIGH18	2.21	8
2011 Tohoku, Japan	9.00	Yonezawa	70	2007 Chuetsu-oki	6.80	Niigata Nishi Kaba District	1.17	12
2003 Hokkaido, Japan	9.00	Shihoro	21	1979 Imperial Valley-06	6.53	Holtville Post Office	0.53	5
2003 Hokkaido, Japan	9.00	Shihoro	27	1992 Landers	7.28	LA - S Grand Ave	2.51	20
2003 Hokkaido, Japan	9.00	Obihiro	20	1999 Chi-Chi, Taiwan-06	6.30	CHY032	2.38	21
2003 Hokkaido, Japan	9.00	Obihiro	28	1979 Imperial Valley-06	6.53	El Centro Array #6	0.47	4
2003 Hokkaido, Japan	9.00	Oiwake	24	1999 Hector Mine	7.13	Mill Creek Ranger Station	2.46	15
2003 Hokkaido, Japan	9.00	Oiwake	26	1999 Chi-Chi, Taiwan	7.62	TCU049	0.46	18
2003 Hokkaido, Japan	9.00	Hayakita	28	1999 Chi-Chi, Taiwan	7.62	TTN026	4.32	21
2003 Hokkaido, Japan	9.00	Hayakita	25	2010 El Mayor-Cucapah	7.20	San Diego - 45th & Orange	4.70	17
2003 Hokkaido, Japan	9.00	Chitose	32	1999 Kocaeli, Turkey	7.51	Arcelik	1.02	5
2003 Hokkaido, Japan	9.00	Chitose	35	1979 Imperial Valley-06	6.53	Brawley Airport	0.58	5
2003 Hokkaido, Japan	9.00	Kuriyama	29	2010 El Mayor-Cucapah	7.20	San Diego - I5 & Laurel	3.50	21
2003 Hokkaido, Japan	9.00	Kuriyama	21	1999 Chi-Chi, Taiwan	7.62	TCU067	0.36	8
μ			56.5					8.6
σ			24.0					6.3
min			10.0					1.0
max			86.0					24.0

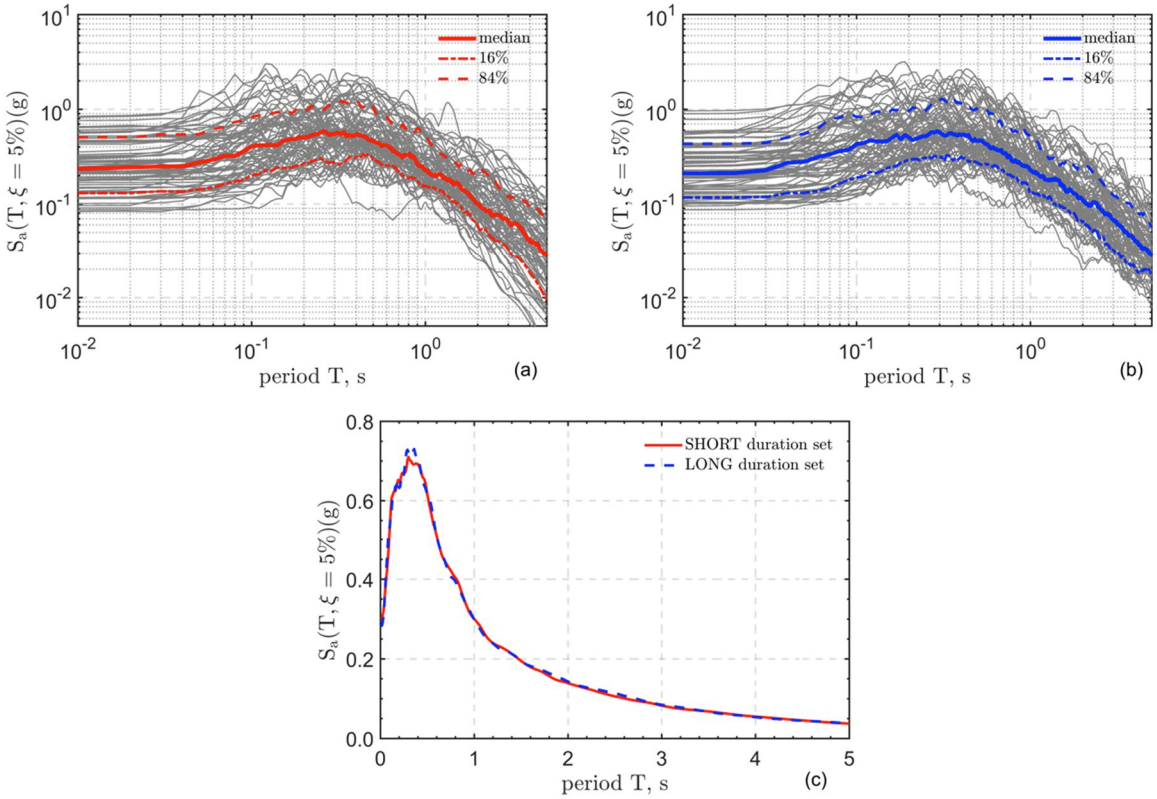

Figure 1. Short duration (a) and long duration (b) ground motion sets log-log median spectra with 16 and 84 percentiles; (c) Median response spectra of the 77 pairs of short and long duration ground motion records.

2.2. Structural systems and modelling assumptions

A large set of steel moment frames designed to Eurocode 3 (**CEN 2005**) and EC8 (**CEN 2004a**), and which have been used by the authors in recent assessments of seismic drift demands (**Bravo-Haro et al. 2018; Tsitos et al. 2018**) have been considered for use in this investigation. The frames were designed based on dissipative behaviour corresponding to high ductility class. In the present study, 50 frames were selected from this set and modelled as equivalent single degree-of-freedom (ESDOF) systems which can account for gravity loads and P-delta effects. In addition, four frames were modelled in detail as two-dimensional multi-degree-of-freedom (MDOF) systems. Both structural modelling approaches were used to carry out extensive incremental dynamic analysis (IDA) in order to examine the effects of ground motion duration by direct comparison of the structural response as subjected to the spectrally equivalent sets of short and long records. A description of the main characteristics of the MDOF and ESDOF systems is given below, while full details and design assumptions of the structures considered are available elsewhere (**Bravo-Haro et al. 2018; Tsitos et al. 2018**)

In the following, the specific structural systems used throughout the paper are described, and the numerical modelling details are outlined further in the relevant section. It should be noted that the following three structural systems are sequentially utilised in this study:

- Single-degree-of freedom (SDOF), with and without degradation, corresponding to classical SDOF oscillators (in Section 3).
- Multi-degree-of-freedom (MDOF) corresponding to full representations of multi-storey frames (in Section 4).
- Equivalent single-degree-of-freedom (ESDOF) with degradation and P-delta effects (i.e., considering gravity loads), corresponding to a refined equivalent system (in Sections 5 and 6).

3. INELASTIC DISPLACEMENT RATIOS

To provide an initial evaluation of the effects of duration through the utilisation of spectrally equivalent ground motion records, a parametric assessment on idealised classical single-degree-of-freedom (SDOF) systems is described in this section. The response is assessed by means of the inelastic displacement ratios (C_R), which are defined as the peak lateral inelastic displacement demand ($\Delta_{inelastic}$) divided by the peak lateral displacement demand (S_d) of an equivalent elastic SDOF system. In this research, inelastic displacement ratios were computed for SDOF systems having 6 levels of lateral strength ratio R which, along with the inelastic displacement ratio C_R, are defined as follows:

$$C_R = \frac{\Delta_{inelastic}}{S_d} \quad (1)$$

$$R = \frac{mS_a}{F_y} \quad (2)$$

where m is the mass of the system, S_a is the acceleration spectral ordinate corresponding to the period of vibration, and F_y is the lateral yield strength. To provide a basis for comparison, a non-degrading bilinear system as well as a stiffness- and strength-degrading model were considered. The non-degrading model considers a post-yield isotropic hardening, while the degrading model adopts the Modified Ibarra-Medina-Krawinkler (ModIMK) bilinear representation (**Ibarra et al. 2005**). This model was experimentally calibrated by **Lignos and Krawinkler (2010)** for reproducing the moment-rotation behaviour of steel components, with local buckling phenomena being the main source of degradation. In order to define the governing monotonic reference backbone curve, an equivalent SDOF idealization of a 7-storey steel moment frame (i.e., C08) was undertaken (**Tsitos et al. 2018**).

The range of periods considered for both hysteretic models was from $T = 0.05s$ to $T = 3.0s$ with intervals of $0.05\ s$, leading to a set of 60 SDOF oscillators. A viscous damping ratio of 5% was assumed. Using the scaling factor as in Equation 3, the short and long duration records were scaled in order to achieve 6 levels of lateral strength ratio R from 1 (elastic) to 6. For each individual nonlinear time history analysis (NTHA), the inelastic displacement ratios C_R were recorded. In this preliminary assessment, 27720 inelastic displacement ratios for each pair of ground motion set and hysteretic system (corresponding to 60 periods of vibration, 77 ground motions and 6 levels of relative strength) were carried out. Therefore more than 100,000 values of C_R were obtained. These inelastic displacement ratios were then grouped by ground motion set, normalized period of vibration and level of relative strength, and processed using simple moving sample means to obtain the central tendency of C_R. The normalised period was used, representing the ratio between the fundamental period (T_1) and the mean period of the ground motion record (T_m), as proposed by **Rathje et al. (1998)**. This normalisation was selected in order to capture the role of the frequency content of the ground motion. The results are depicted in Figure 2 to Figure 5.

Figure 2 (a) and (b) clearly show that for the case of non-degrading bilinear hysteretic models, the differences are generally insignificant between the mean C_R of the short duration set (left) and the long duration set (right). This is valid for both the distribution and amplitude of C_R. Besides, the values of C_R begin converging to unity (i.e., equal displacement rule) at the same normalised period ($T_1/T_m \approx 2$), indicating that the duration is not playing a significant role in inelastic displacements for non-degrading systems. In contrast, Figure 3 (a) and (b) show a visible relative increase in C_R tendency when hysteretic degrading systems are used. This relative increase is greater for higher levels of lateral strength (R). The convergence point of C_R to unity is also shifted to $\mathrm{T_1/T_m} \approx 3.5$. This shows the notable influence of long ground motion duration with increased inelastic displacement demand in degrading systems.

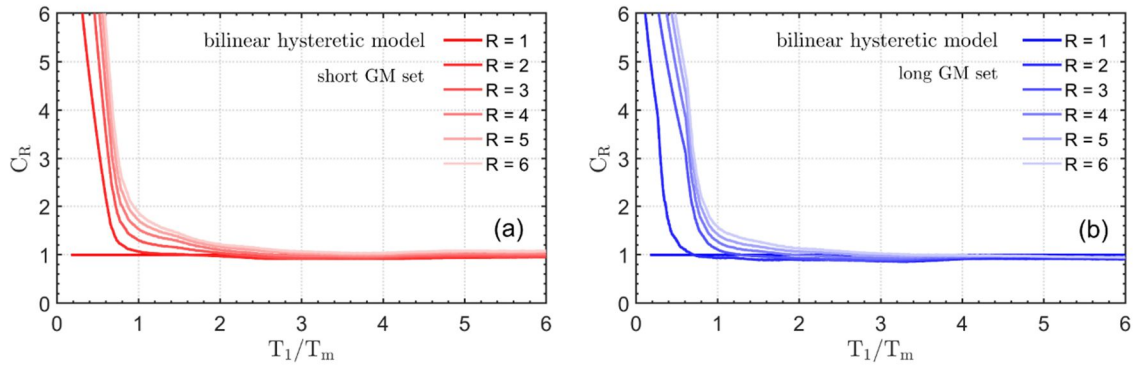

Figure 2. Mean maximum inelastic displacement ratio C_R as a function of T_1/T_m for non-degrading bilinear systems: (a) short duration set and, (b) long duration set.

For direct comparison, Figure 4 (a) and (b) show ratios of $\mathrm{C_R}$ due to both sets of records. The tendency of C_R is presented in this case in terms of the fundamental period (T_1) of the oscillator since the spectrally equivalent sets have different mean periods T_m. Irrespective of *R*, the discrepancy in the prediction of C_R for short and long duration records is negligible. In contrast, for degrading hysteretic systems, the values of C_R due to the long duration set are consistently higher than those for the short duration. The latter is valid for all levels of lateral strength except the elastic level (i.e., $\mathrm{R} = 1$) and for periods less than $T_1 \approx 1.5s$. Finally, a direct comparison between the bilinear non-degrading and degrading models is presented in Figure 5 (a) and (b) by the ratio of $\mathrm{C_R}$ computed from both sets of records. As indicated, the inelastic displacement demands are higher in degrading models in all cases including for short duration earthquakes. More significant differences are observed for higher values of R; for instance, for a $T_1/T_\mathrm{m} = 1$ and $R = 6$, an average value of $\mathrm{C_R}$ about 1.6 times higher for degrading system is obtained for short records; this ratio increases more for long duration records, where the corresponding ratio is about 2.8 times in degrading systems. It is evident that a wider range of normalised periods exhibits values higher than unity (C_R>1) for the long duration set.

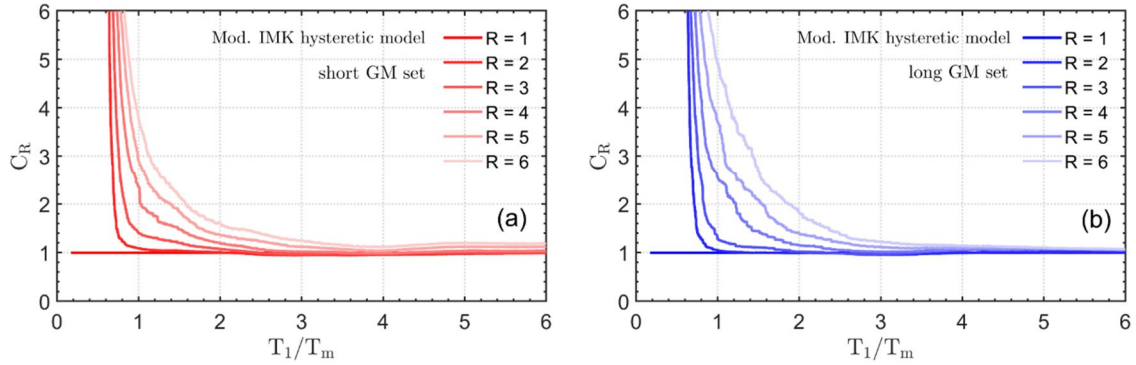

Figure 3. Mean maximum inelastic displacement ratio C_R as a function of T_1/T_m for degrading systems: (a) short duration set and, (b) long duration set.

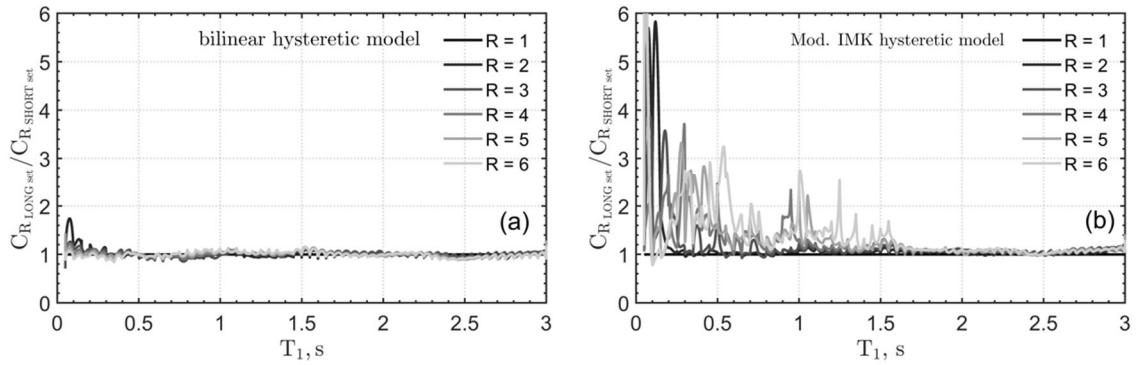

Figure 4. Mean ratio of long duration set ($C_{R_{LONG\,set}}$) to short duration set ($C_{R_{SHORT\,set}}$) as a function of T_1 for: (a) non-degrading systems, and (b) degrading systems.

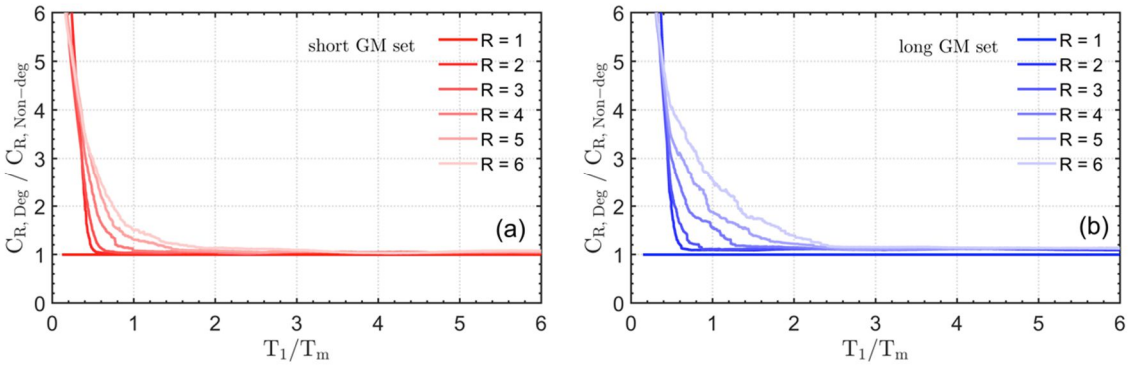

Figure 5. Mean ratio of degrading systems ($C_{R,Deg}$) to non-degrading systems ($C_{R,Non-deg}$) as a function of T_1/T_m for: (a) short duration, and (b) long duration ground motion sets.

4. COLLAPSE FRAGILITY CURVES

The moment resisting frame consists of 3 bays (with a bay span of 6 m) and 3, 5, 7 or 9 stories. The first storey has a height of 4.5 m, whereas the upper stories have a typical height of 3.5m. Figure 6. shows a plan and elevation of the typical structural system of the buildings, which encompasses three lateral resisting moment frames in the in-plane direction, while braced frames provide lateral load resistance in the orthogonal direction. For brevity,

Table **2** gives a summary of the design details and relevant structural characteristics for only the four frames that are fully characterised as two-dimensional MDOF in this section. As noted in previous studies, capturing the effect of earthquake duration in collapse capacity assessments, requires numerical models that represent accurately the structural behaviour at large nonlinear deformations (**Chandramohan et al. (2016)**. This issue is addressed in Section 3 of this paper, where the inability of non-degrading numerical models to characterise high nonlinear deformations was quantified and discussed. Therefore, the multi-storey frames were modelled using the open-source software OpenSEES (**McKenna (2011)** following a lumped plasticity approach, which is able to consider the cyclic and in-cycle stiffness and strength degradation phenomena for the steel sections.

The structural model employed is constructed from rotational springs, used to idealise the plastic hinges at the ends of beams and columns, which are characterised by the regression relationships proposed by **Lignos and Krawinkler (2010)**, and subsequently adopted in the PEER/ATC-72 report (**ATC 2010**). For the case of columns, the yield moments of the idealised plastic hinges were computed by using an interaction curve, where axial load were calculated based on first order analysis. Column web panel zones were considered for both structural models, and shear-distortion behaviour using zero-length elements was characterised according to the tri-linear hysteretic model proposed by **Gupta and Krawinkler (1999)**. Structural damage is accounted for through the cumulative hysteretic energy dissipated by the plastic hinges which is used to compute the rate of strength and stiffness degradation through the inelastic cycles. This is directly reflected in higher lateral inelastic demand. Further details of the numerical modelling approaches can be found elsewhere (**Bravo-Haro et al. 2018**)

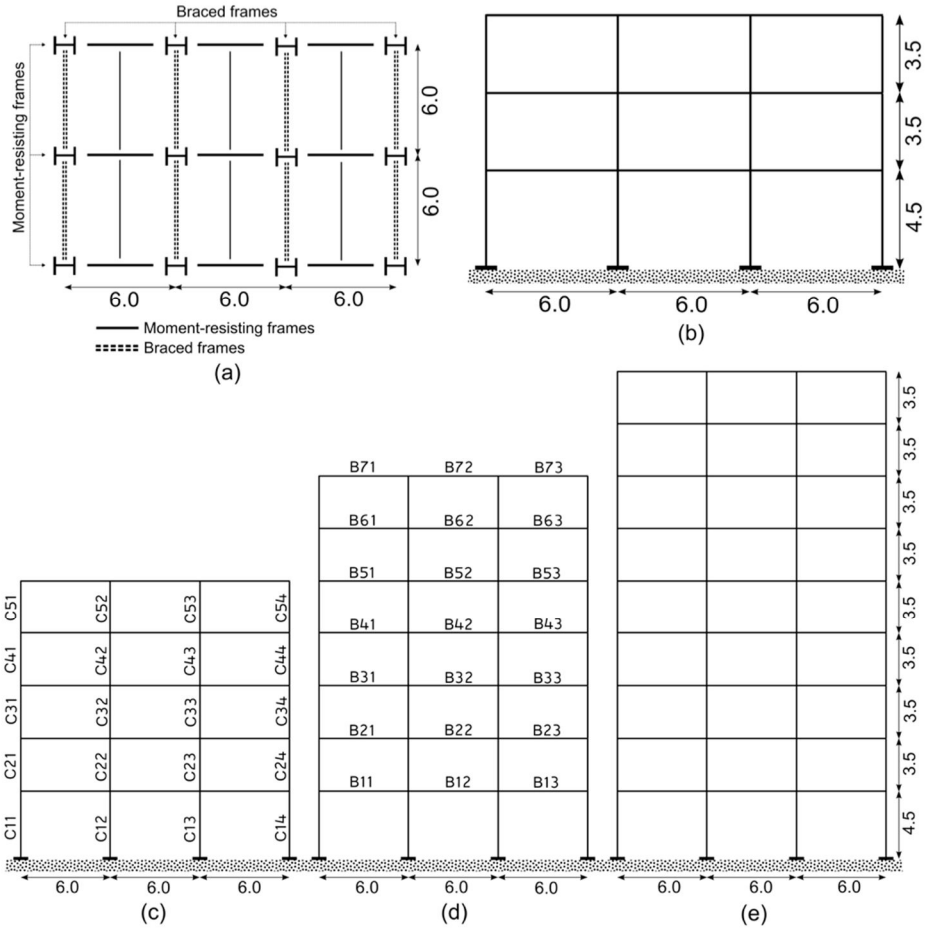

Figure 6. Structural configurations: (a) typical plan, (b)-(e) schematic elevation of the 4 frame sets fully modelled as MDOF (standard notation for beams and columns illustrated in (c) and (d), respectively).

Table 2. Details and characteristics of the four frames fully modelled as MDOF systems

Frame ID	Structural steel profiles	Structural properties				
	Beams (first row) and Columns (second row) from first storey upwards	T_1, s	T_2, s	H, m	N_s	N_b
A05	IPE330, IPE330, IPE300	1.00	0.28	11.50	3.00	3.00
	HEB340, HEB340, HEB340					
B10	IPE360, IPE360, IPE330, IPE330 IPE300	1.44	0.45	18.50	5.00	3.00
	HEB400, HEB400, HEB400, HEB400, HEB300					
C08	IPE400, IPE400, IPE400, IPE400, IPE400, IPE400, IPE300	1.66	0.54	25.50	7.00	3.00
	HEB450, HEB450, HEB450, HEB400, HEB400, HEB400, HEB300					
D05	IPE500, IPE500, IPE500, IPE500, IPE500, IPE450, IPE450, IPE400, IPE360	1.51	0.52	32.50	9.00	3.00
	HEM500, HEM500, HEM500, HEM450, HEM450, HEM450, HEM400, HEM400, HEM400					

In this section, selected results illustrating the influence of ground motion duration on multi-degree-of-freedom systems (MDOF) are briefly presented to highlight key trends. For this purpose, the four steel multi-storey frames (described in Table 2) are subjected to IDA to develop collapse fragility curves, for both sets of ground motion records. In all cases, the collapse limit is defined by dynamic instability corresponding to the flattening of the IDA curves. As noted before, the 4 structural systems represent typical steel moment frames designed to European code procedures, comprising four different heights, namely 3, 5, 7 and 9 stories. In addition, IDA is carried out considering a third *duration-blind* earthquake records set, included in the FEMA P-695 (2009) seismic report. This set has been considered primarily to gain further understanding on the effects of ground motion duration and to place the observations obtained herein within the context of current state-of-the-art seismic guidelines. It is important to note that direct comparison between the results from the ground motion records with an equivalent spectral

shape and the FEMA set is incorrect due to the influence of frequency content and spectral amplitude. To mitigate this issue, a fourth set of 154 records including short and long duration ground motions (referred to as a "global set") is considered so that a more rational comparison is obtained.

The resulting fragility curves are shown in Figure 7 (a) – (d), rather than the detailed IDA results, for brevity. As shown, the median probability of collapse is consistently higher for the long records compared to the short records, for all the selected structures. For the same frame, lower ground motion intensity instigates structural collapse for the case of long duration records. The decrease in median collapse capacity due to the duration is shown individually in the plots for each frame. Overall, direct comparison of both sets of records shows collapse capacities that are $9-24\%$ lower due to longer duration earthquakes. A summary of the median collapse capacities obtained from the fragility curves for the 4 buildings, due to the action of each record set is presented in Table 3, along with the decrease or increase in the median collapse capacity for the short duration set, when long duration or FEMA P-695 sets are considered.

The estimated collapse fragility curves due to the seismic excitation of FEMA P-695 ground motion set tend to be closer to the case of spectrally equivalent short duration set. The results indicate that the structural fragility of the frames is consistently higher due to the effect of the global set of records, with respect to the response of the FEMA set. Therefore, the difference between the structural fragility when long duration sets are compared to the duration-blind set is even more significant as shown in Table 3. This reinforces the observations noted above on the lack of guidance on ground motion duration effects in current seismic guidelines. The structural collapse analysis obtained by using the FEMA P-695 records appears to be conservative with respect to the spectrally equivalent sets. It is however important to note that the FEMA P-695 set of records is not spectrally equivalent to the short and long duration sets. This MDOF collapse analysis shows that in the new generation of performance-based guidelines, the explicit inclusion of earthquake duration, such as in the case of the global set (i.e., short and long) of this section, would represent a notable improvement in the procedures.

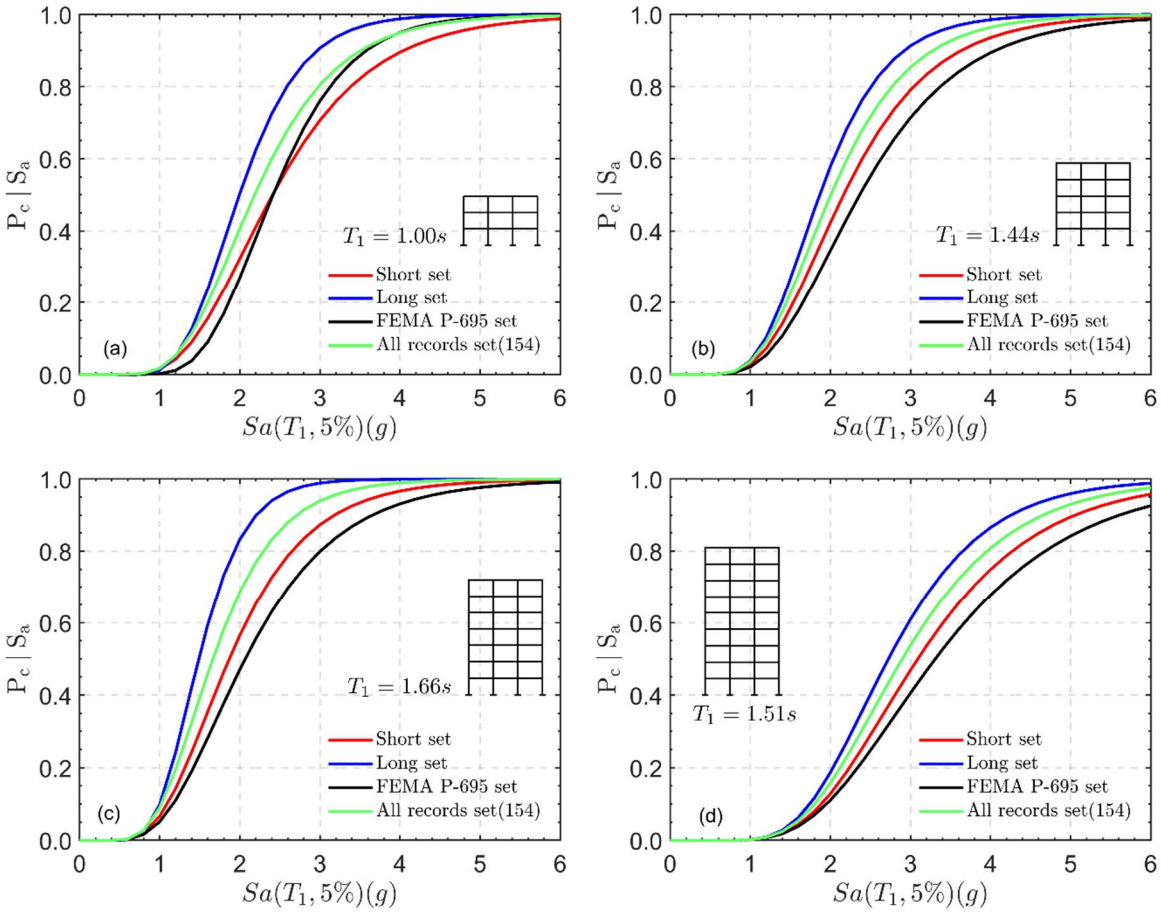

Figure 7. Collapse fragility curves for 4 multi-storey frames (selected from the study of **Tsitos et al.**

2018): (a) A05, (b) B10, (c) C08 and (d) D05 due to short duration (red lines), long duration (blue lines), FEMA set (black lines), and global set (green lines) of ground motion records.

Table 3. Summary of collapse fragility functions for each building under the three ground motion sets.

	Median collapse capacity, $S_a(T_1)$				Ratio, %		
Frame ID	Short	Long	FEMA P-695	Global	Long/Short	FEMA/Short	Global/FEMA
A05	2.60	2.00	2.60	2.20	-23.08	0.00	-15.38
B10	2.20	2.00	2.40	2.20	-9.09	9.09	-8.30
C08	2.10	1.60	2.20	1.80	-23.81	4.76	-18.18
D05	3.20	2.80	3.40	3.00	-12.50	6.25	-11.76

5. SENSITIVITY ASSESSMENTS

5.1. Equivalent single-degree-of freedom systems

The N2 method adopted in Eurocode 8 (**CEN 2004a**) was largely followed to obtain the equivalent structural properties of the ESDOF systems from the corresponding MDOF. However, as the EC8 version of the method is limited to perfectly plastic systems, an updated linear fit of the static pushover capacity curve for equivalent SDOF analysis as proposed by **De Luca et al. (2013)**, was used herein. Both the structural members in MDOF systems and the rotational spring in ESDOF systems employed the degrading modified Ibarra-Medina-Krawinkler (modified IK) hysteretic bilinear model (**Ibarra et al. 2005; Lignos and Krawinkler 2010**). The modified IK model takes into account the cyclic degradation through a rate of deterioration (Λ), which is controlled by a rule developed by **Rahnama and Krawinkler (1993)** on the basis of the hysteretic energy dissipated during cyclic loading demand of the component. The parameter Λ can be individually defined to characterise four cyclic deterioration modes: basic strength, post-capping strength, unloading stiffness, and reloading stiffness deterioration. However, former calibration studies (**Lignos and Krawinkler 2007; 2010**), have shown that for steel components, this individual refinement does not lead to significant model improvements. Therefore, the same rate of cyclic deterioration is used herein for all the modes and is henceforth referred to as Λ.

Since Λ is particularly important in this study, its incorporation in the ESDOF systems is carried out through a calibration process based on cyclic pushover analysis of the multi-degree-of-freedom (MDOF) systems, and used as a target response for the subsequent cyclic pushover analysis of the ESDOF system. This methodology provides an equivalent cyclic deterioration ratio to be used with the ESDOF systems and, for simplicity, this equivalent ratio is still referred to as Λ. In the calibration process, the mean squared error of the cyclic force-deformation response was minimized in order to find the near-optimal value of the equivalent rate of cyclic deterioration. As a typical illustration of this methodology, which was undertaken on 50 moment resisting frames fully modelled as MDOF systems, the MDOF monotonic and ESDOF cyclic pushover curves for a selected case of a 3-storey frame (Frame A02) are shown in Figure 8. For this particular frame, the value of the equivalent cyclic deterioration rate obtained corresponds to $\Lambda = 11$.

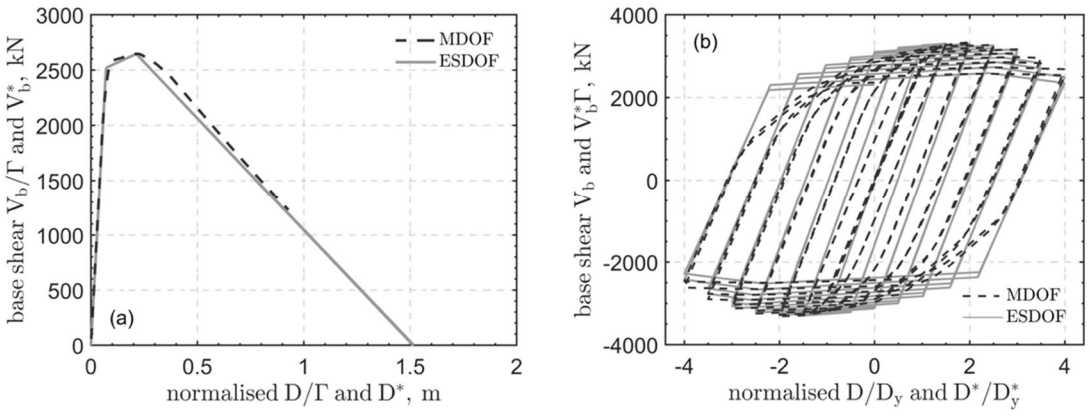

Figure 8. Calibration of equivalent single-degree-of-freedom model (ESDOF) for Frame A02: (a) monotonic pushover, and (b) cyclic pushover.

The relevant structural parameters of the equivalent single-degree-of-freedom systems are listed in Table 4. In the table, T_1 corresponds to the equivalent fundamental period of vibration, N_s is the number of stories, H is the total height of the building in meters, τ is the global lateral stiffness determined as the ratio between T_1 and N_s. The calibrated equivalent rate of cyclic degradation corresponds to Λ, the modal participation factor is Γ, and V_1 is the base shear of the original frame at first yielding obtained through first-mode lateral static pushover. Lastly, M is the total seismic mass of the original system. The ESDOF models representing the set of 50 multi-storey frames are used in the current and subsequent sections of this paper.

Table 4. Details and characteristics of the ESDOF systems

N°	Frame ID	T_1, s	N_s	H, m	τ	Λ	Γ	V_1, kN	M, ton
1	A01	0.53	3	11.50	0.18	14.10	1.285	1617.36	208.11
2	A02	0.40	3	11.50	0.13	11.00	1.295	2766.67	213.42
3	A03	0.74	3	11.50	0.25	19.88	1.286	922.64	205.90
4	A04	0.41	3	11.50	0.14	19.60	1.278	2238.09	213.34
5	A05	1.00	3	11.50	0.33	15.67	1.291	656.76	204.14
6	A06	0.84	3	11.50	0.28	14.00	1.319	824.65	204.78
7	A07	0.62	3	11.50	0.21	9.64	1.289	1429.84	206.94
8	A08	0.75	3	11.50	0.25	14.44	1.302	985.91	206.03
9	B01	0.40	5	18.50	0.09	8.50	1.364	4211.54	369.90
10	B02	0.79	5	18.50	0.16	11.00	1.397	1675.89	362.20
11	B03	0.97	5	18.50	0.20	14.40	1.348	1339.09	355.05
12	B04	0.52	5	18.50	0.11	8.17	1.412	3614.23	365.13
13	B05	0.93	5	18.50	0.19	11.40	1.387	1292.29	358.06
14	B06	0.98	5	18.50	0.20	13.45	1.382	1262.52	355.24
15	B07	1.10	5	18.50	0.22	16.95	1.351	1054.80	354.19
16	B08	0.79	5	18.50	0.16	13.65	1.379	1794.46	358.82
17	B09	0.52	5	18.50	0.10	8.25	1.422	3631.40	365.10
18	B10	1.44	5	18.50	0.30	17.93	1.352	685.83	350.87
19	B11	1.13	5	18.50	0.23	15.90	1.362	1034.18	352.73
20	B12	0.87	5	18.50	0.17	11.50	1.408	1640.90	355.60
21	B13	1.16	5	18.50	0.23	14.63	1.381	936.96	352.86
22	B14	1.16	5	18.50	0.23	15.75	1.350	1009.88	325.70
23	B15	1.11	5	18.50	0.22	14.80	1.352	1086.45	353.73
24	C01	0.89	7	25.50	0.13	14.50	1.333	2231.09	517.26
25	C02	1.05	7	25.50	0.15	15.10	1.353	1796.04	514.26
26	C03	1.05	7	25.50	0.15	14.00	1.328	1787.06	513.29
27	C04	0.97	7	25.50	0.14	13.44	1.353	2120.29	514.04
28	C05	1.13	7	25.50	0.17	15.93	1.382	1622.55	511.60
29	C06	1.35	7	25.50	0.19	16.00	1.387	1254.00	502.61
30	C07	0.96	7	25.50	0.14	14.16	1.400	2133.70	510.08
31	C08	1.66	7	25.50	0.25	15.56	1.334	902.75	499.19
32	C09	0.67	7	25.50	0.10	7.93	1.407	3556.06	518.83
33	C10	1.50	7	25.50	0.21	13.07	1.363	1166.93	500.51
34	C12	1.52	7	25.50	0.22	12.53	1.365	1160.06	499.84
35	C13	1.13	7	25.50	0.16	13.70	1.382	1647.07	511.60
36	C14	1.37	7	25.50	0.20	13.60	1.416	1275.96	501.81
37	C15	1.02	7	25.50	0.15	11.35	1.453	2023.55	508.98
38	C16	1.04	7	25.50	0.15	12.35	1.440	2040.56	508.68
39	D01	1.04	9	32.50	0.12	18.60	1.323	3386.00	671.92

40	D02	1.25	9	32.50	0.14	14.92	1.359	2637.89	666.75
41	D03	1.31	9	32.50	0.15	14.16	1.362	2475.81	665.69
42	D04	1.39	9	32.50	0.15	14.36	1.398	2300.64	663.81
43	D05	1.51	9	32.50	0.17	15.28	1.367	1962.37	662.53
44	D06	1.77	9	32.50	0.20	13.84	1.347	1504.55	660.04
45	D08	0.92	9	32.50	0.10	13.76	1.447	3947.13	672.00
46	D10	1.28	9	32.50	0.14	18.80	1.342	2384.75	666.50
47	D11	0.99	9	32.50	0.11	14.90	1.405	3738.52	671.19
48	D12	1.05	9	32.50	0.12	16.60	1.389	3509.21	670.48
49	D14	1.91	9	32.50	0.21	13.64	1.350	1438.30	647.40
50	D15	1.36	9	32.50	0.15	14.28	1.395	2393.91	664.15

5.2. Results

In this subsection, a more refined equivalent single degree of freedom (ESDOF) model that can capture the effect of gravity load is used. The mechanical model shown in Figure 9 (a) corresponds to an inverted pendulum with mass (m) at its tip, and the rod is a massless element pinned at the base. The properties of the moment-rotation structural model are assigned to a rotational spring at the base. Viscous damping is considered using a rotational dashpot damper acting in parallel with the main rotational spring. Likewise, Figure 9 (b) shows the quadrilinear monotonic moment-rotation backbone curve that controls the response of the hysteretic law assigned to the rotational spring (**Ibarra et al. 2005**; **Lignos and Krawinkler 2010**). The 6 parameters that define the model are the yield moment (M_y), the post-yield hardening slope (α_h), the capping rotation (θ_p), the post-capping softening negative slope (α_{pc}), the residual moment plateau - defined as a proportion (r) of the yield moment and the ultimate rotation (θ_u). In order to perform a sensitivity analysis of each parameter at a time, a *reference model* is set considering the structural properties of the 7-storey (i.e., C08) frame used in Section 3.

To examine the influence of key parameters on the behaviour due to long and short duration ground motions, each parameter is varied within typical values covered in the steel moment frames, with respect to the reference model, with all the other parameters retaining their values. A recent study (**Bravo-Haro et al. 2018**) in which 50 steel moment resistant frames were investigated was used as a benchmark to select the parameter ranges. Each variable is assessed using incremental dynamic analysis (IDA) procedures (**Vamvatsikos and Cornell 2002**) utilising both sets of ground motion records. The results are presented in terms of the reduction in the spectral acceleration demand as a direct ratio of the long to short duration sets, as illustrated in Figure 10 for the reference model. The collapse limit is defined by dynamic instability corresponding to the flattening of the IDA curves, which corresponds to the same criterion used in Section 4.

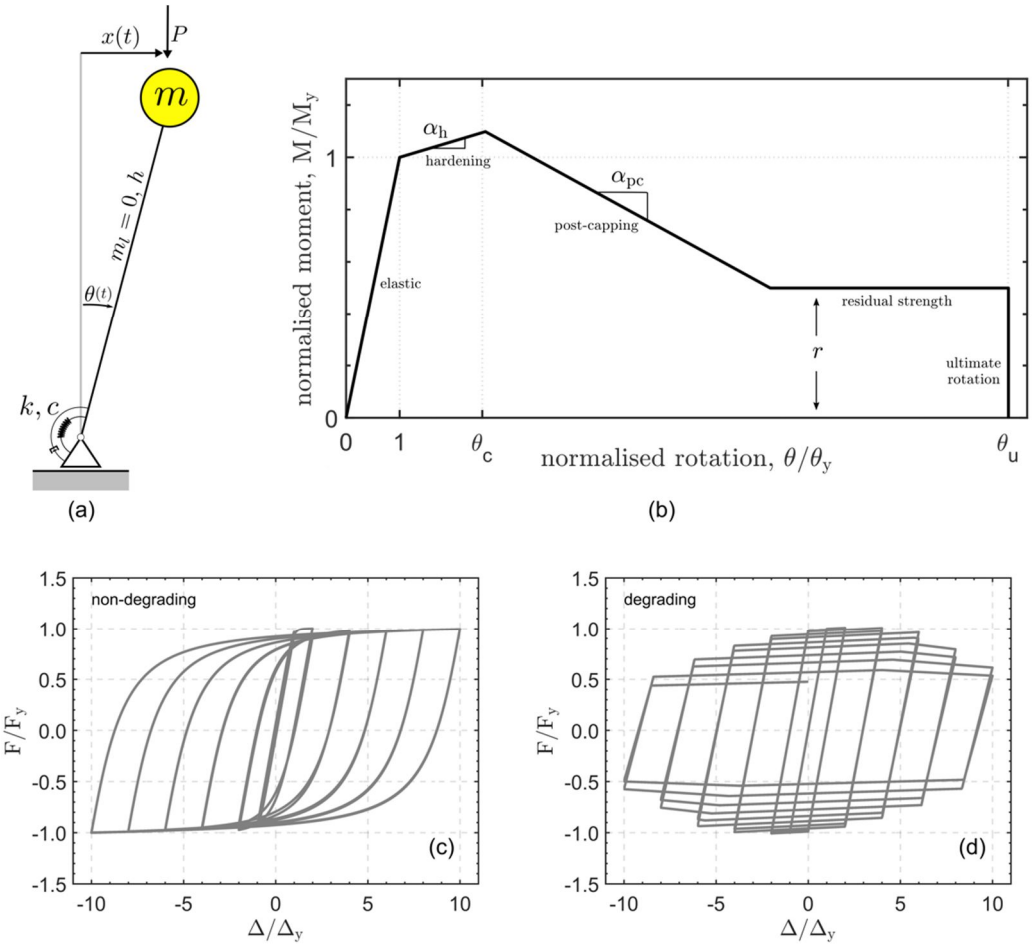

Figure 9. (a) Mechanical model of the ESDOF system; (b) Normalised moment-rotation backbone curve of the hysteretic spring assigned to the base of the mechanical model; (c) Non-degrading and (d) degrading hysteretic material models assigned to the spring.

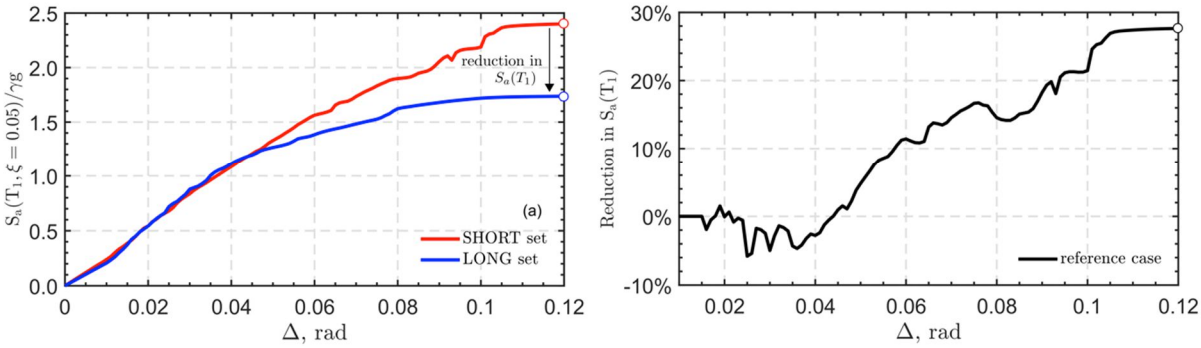

Figure 10. Mean IDA curves due to both ground motion sets for the reference model (a), and percentage reduction in spectral acceleration obtained from the mean IDA curve of the long set with respect to the short duration set (b).

The results for the 6 individual parameters are shown in Figure 11 to Figure 13, noting that each ground motion set contains 77 individual records. Figure 11 (a) defines the effect of M_y on the influence of ground motion duration, which is most evident at the structural collapse limit. An increase of the yield moment produces a lower effect due to the ground motion duration. In contrast, a similar decrease of yield moment results in a noticeable increase in the influence of duration. At earlier stages of drift demand, the differences are negligible. In the case of the post-yielding hardening slope α_h, as depicted in Figure 11 (b), a significant increase in α_h leads to a higher influence for duration, while a decrease of this effect is observed when α_h is reduced. However both changes are delimited by a range of 10% of the seismic capacity due to the ground motion duration. It is also interesting to note that for lower drift demands, a reversal in behaviour occurs until dynamic instability is approached.

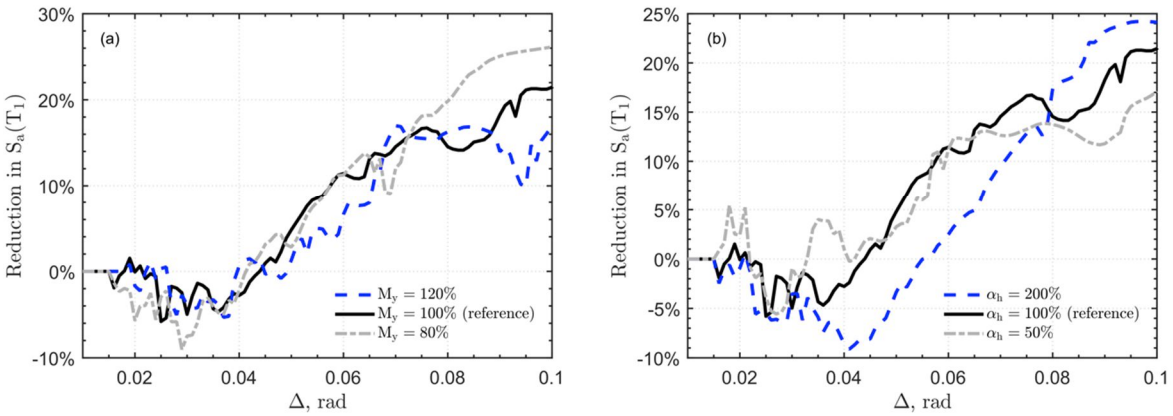

Figure 11. Sensitivity of the IDA to the spectral acceleration demand ratios: (a) yield moment $\mathrm{M_y}$, and (b) post-yield hardening slope α_h.

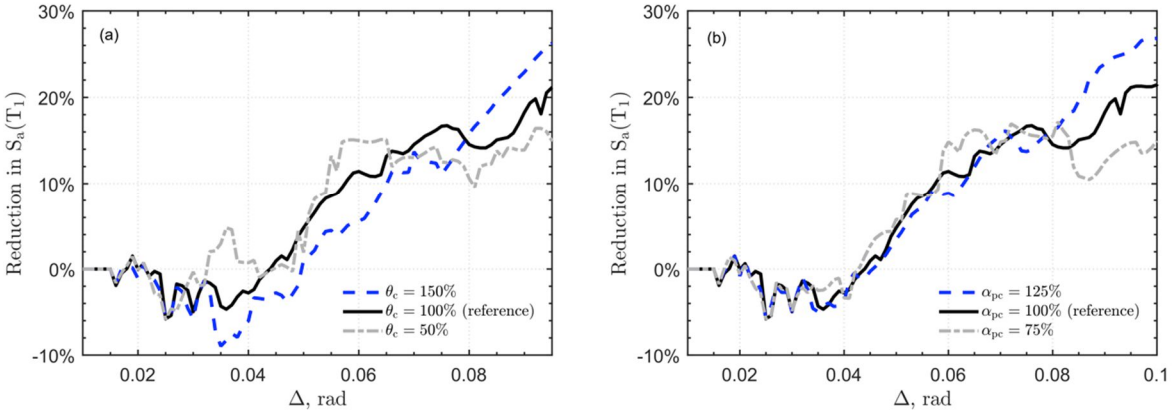

Figure 12. Sensitivity of the IDA to the spectral acceleration demand ratios: (a) capping rotation, θ_c, parameter and (b) post-capping softening negative slope, α_{pc}, parameter.

The effect of θ_c on the influence of ground motion duration appears to be relatively insignificant as shown in Figure 12 (a). An increase of 50% in the capping capacity corresponds to a 3% reduction in the global influence of duration at the collapse level. In earlier phases of drift demand, the response of the 3 cases considered is not notably different. The case of post-capping softening negative slope (α_{pc}) is shown in Figure 12 (b) where a practically unchanged response is observed until it reaches the collapse limit where a 4% change occurs for both variations, with a steeper negative slope of α_{pc} indicating a more significant influence of ground motion duration. On the other hand, with reference to Figure 13 (a), the residual strength ratio r shows a marginal effect on the influence of duration at the collapse limit, since both variations tend to oscillate around the reference case. However, at lower drifts, up to 10% change can be observed. Finally, an increase of the ultimate rotation (θ_u) does not appear to affect the seismic response due to duration. In contrast, a similar reduction in θ_u (i.e., -33% from the reference case) reduces the influence of duration by around 8%.

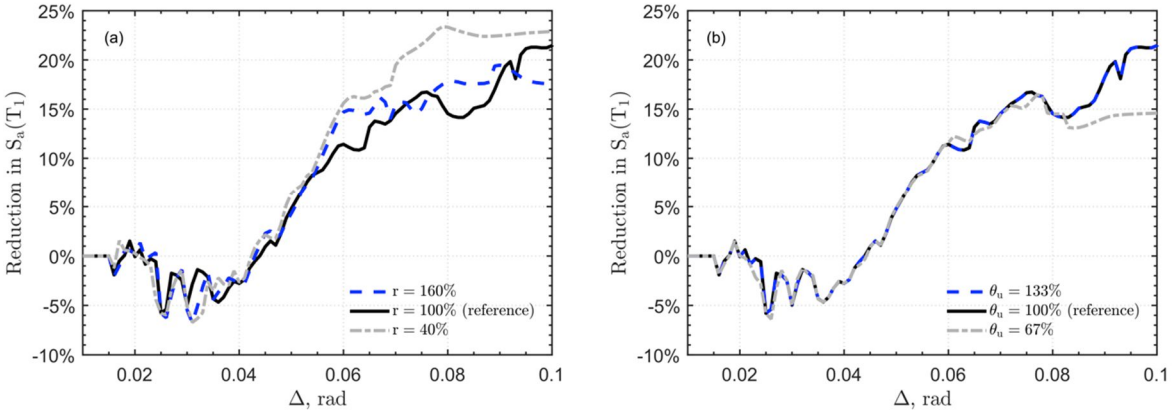

Figure 13. Sensitivity of the IDA to the spectral acceleration demand ratios: (a) residual moment strength ratio r, and (b) ultimate rotation θ_u.

A sensitivity assessment is also carried out on the influence of the cyclic degradation rate. The reference case is maintained, with a cyclic deterioration rate of 15.56, whilst lower and higher values were assumed to cover ranges observed from detailed studies on steel multi-storey frames (**Bravo-Haro et al. 2018**). To this end, it should be noted that the rate of cyclic degradation of a system (**Ibarra et al. 2005**) is fully defined by the structural typology, hence the upper values of Λ (i.e., lower cyclic deterioration rate) are usually reached in highly ductile designs with small levels of over-strength. In contrast, low values of Λ reflect more stocky and less ductile systems with lower periods. On this basis, Figure 14 shows the percentage reduction in spectral acceleration demand due to ground motion duration for all considered cases of Λ. The influence is more evident when the system reaches dynamic instability or collapse level, exhibiting considerable differences of up to 25% due to the ground motion duration. At this limiting stage, the higher the rate of cyclic deterioration (i.e., lower values of Λ), the higher the influence of duration, reaching up to almost 40% reduction in capacity.

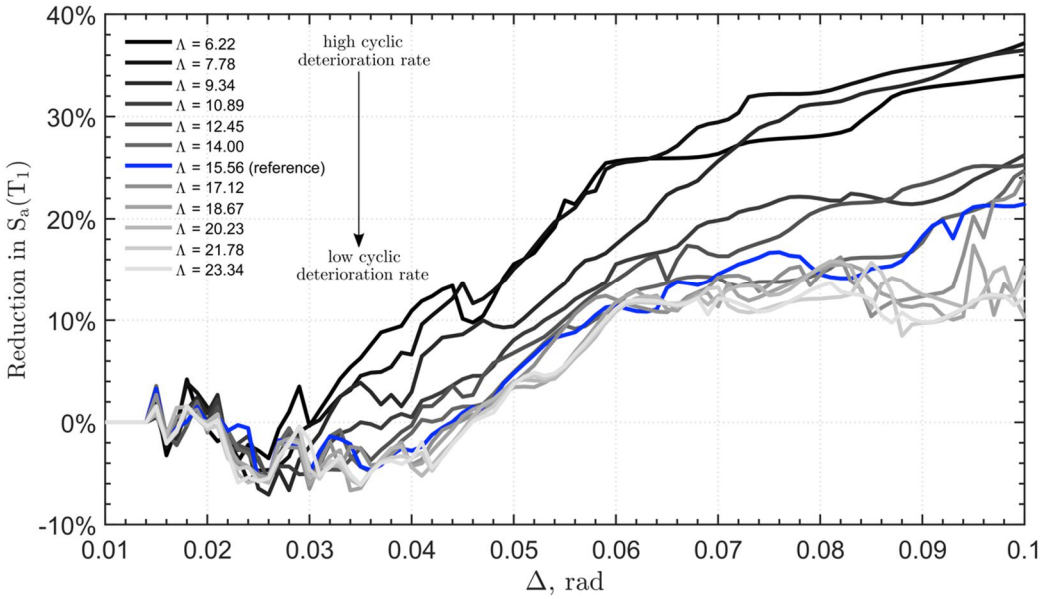

Figure 14. Change in median spectral acceleration estimated by the long duration set with respect to the short duration through IDA, for different values of equivalent cyclic deterioration (Λ).

It is interesting to observe from Figure 14 that the capacity is affected at modest demand stages typically associated with design levels. This is examined further in Figure 15 and Figure 16 for such levels of lateral drift demand. Figure 15 (a) and (b), at inter-storey drift (Δ) of 30 and 40 mrad, respectively, show a reversibility trend, observed before for the 6 backbone parameters, when Λ corresponds to the reference model. This is reflected in an almost 5% reduction in spectral acceleration demand for the short duration set for values of Λ near the reference case. However, when higher rates of deterioration are considered, up to 12% reduction in spectral acceleration demand can be reached (Figure 15 (b)).

For higher levels of demand, the influence of duration is evident from Figure 16 (a) and (b) for 50 mrad and collapse level of drift demand, respectively. For high rates of deterioration up to 15% and 40%, changes due to duration are notable. At collapse level, when rates of cyclic deterioration are smaller (i.e., higher values of Λ), a lower bound is reached and maintained around 8%. This is in broad agreement with findings by **Chandramohan et al. (2016)** which was attributed to cyclic ratcheting effects where dynamic instability is reached due to large lateral drifts induced by $P-\Delta$ effects (**Gupta and Krawinkler 2000**).

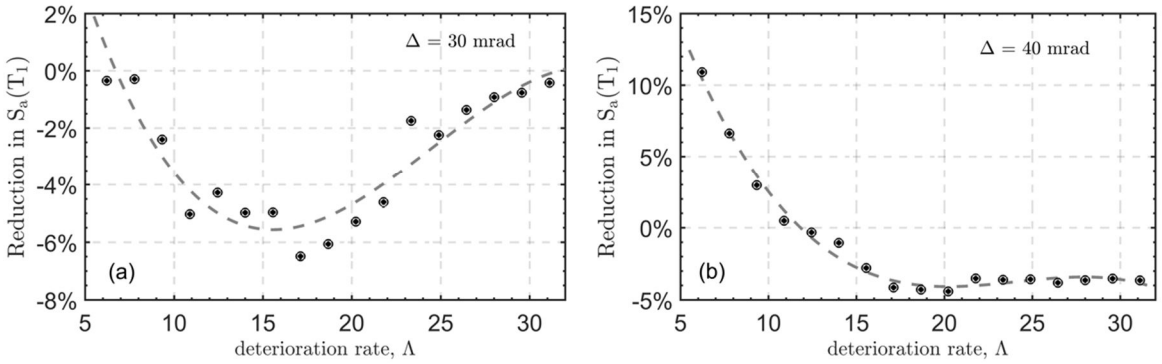

Figure 15. Variation in median spectral acceleration demand estimated from the long duration set with respect to the short duration set, for different levels of lateral demand: (a) $\Delta = 30$ mrad, and (b) $\Delta = 40$ mrad.

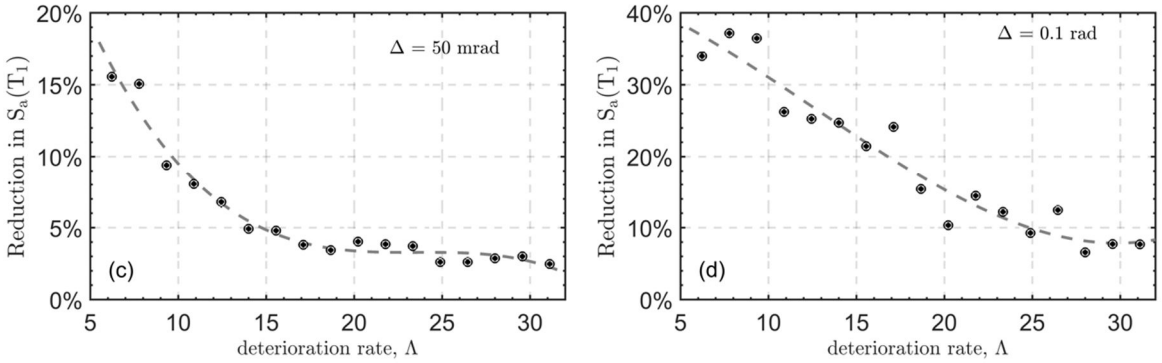

Figure 16. Variation in median spectral acceleration demand estimated from the long duration set with respect to the short duration set, for different levels of lateral demand: (a) $\Delta = 50$ mrad, and (b) $\Delta = 0.1$ rad.

6. COLLAPSE CAPACITY SPECTRA (CCS)

6.1. Preliminary assessment

The influence of ground motion duration is clearly significant at the collapse level in most cases, and particularly when degrading models are used. This section presents a brief initial study on the influence of duration for a wide range of periods. For this purpose, the collapse capacity spectrum (CCS), firstly introduced by **Adam and Jäger (2012)**, is used, and the same multi-storey frames employed in Section 5 above are considered. The construction of the CCS requires the computation of the relative intensity measure denoted collapse capacity (CC) of each individual ground motion record and is defined as follows.

$$CC = \frac{S_a(T_1)_{collapse}}{g\gamma} \tag{3}$$

Where $S_a(T_1)_{collapse}$ corresponds to the 5%-damped spectral acceleration at the fundamental period of

the structure, g is gravity constant and γ is the base shear coefficient (i.e. ratio of yield strength to seismic weight). By considering the normalisation by $g\gamma$, the relative intensity measure resembles the conventional strength reduction factor R for systems without overstrength. The procedure is based on a series of IDA for a set of fixed structural properties. Using the same ESDOF model introduced in Section 5, and fixing the viscous damping parameter (ξ) to 0.05 as well as the backbone curve parameters and cyclic rate of deterioration, the collapse capacity (CC) is plotted against the varying fundamental period of the equivalent system (T). The outcome is denoted as the collapse capacity spectrum for an individual record. To illustrate this, Figure 17 (a) depicts the resulting IDA curve of the system when the initial period is tuned to be $\mathrm{T} = 2.35\mathrm{s}$, and only one individual record is used (in this case # 15 of the long duration set). Subsequently, the CCS is shown in Figure 17 (b) for a range of 80 initial periods (from $0.05\mathrm{s}$ to 4.0s with a step of $0.05\mathrm{s}$) using the same individual record. The figure indicates the corresponding CC values obtained for the system with an initial period of 2.35s as a reference.

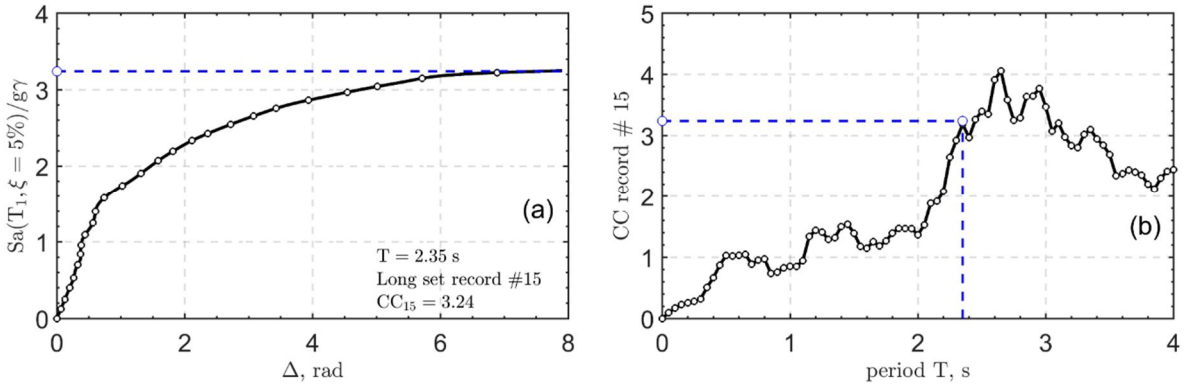

Figure 17. (a) Estimation of collapse capacity for a single ground motion (record #15 of the long duration set); (b) Individual collapse capacity spectrum due to a single ground motion record.

The CCS due to both record sets is depicted in Figure 18, showing the median as well as the 16th and 84th percentile values. A higher concentration of the individual records in lower spectral acceleration is clear for the long duration set, which results in lower dispersion around the central tendency. The median CCS curves are plotted together in Figure 19 (a), and are contrasted with the median CCS obtained from the ground motion set from FEMA P695 (2009) which are duration-independent. This comparison does not comply with the assumption of 'spectral equivalence', yet it illustrates the lack of duration effects in current seismic code procedures. The resultant median CCS from the FEMA P695 set shows a similar behaviour to that obtained for the short duration set. On the other hand, Figure 19 (b) shows the reduction in median CCS obtained from the short duration set divided by that from the long duration set. This percentage ratio indicates considerable differences in the estimation of collapse capacity throughout the range of main periods, with an average plateau of 30% reduction in the CCS due to ground motion duration for periods higher than $0.7s$.

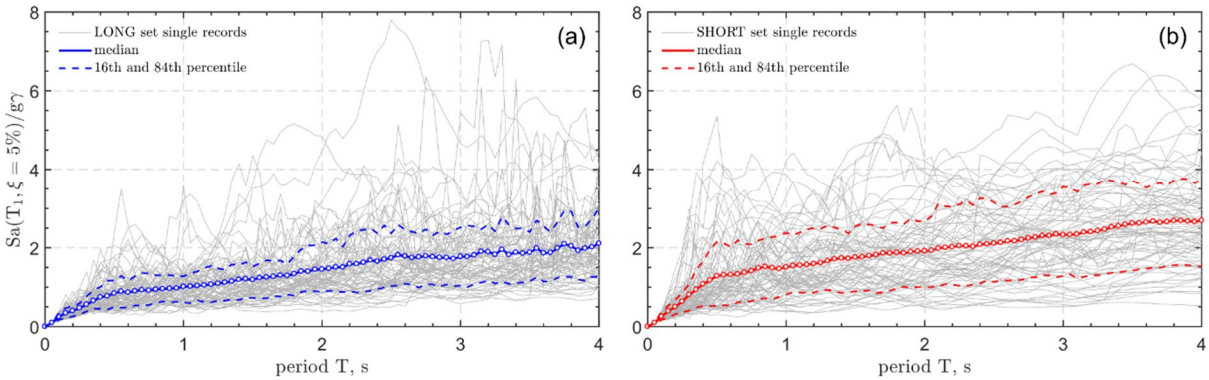

Figure 18. Collapse capacity spectra due to the long (a) and short (b) duration sets of ground motion records, and the corresponding median, 16th and 84th percentile collapse capacity spectra.

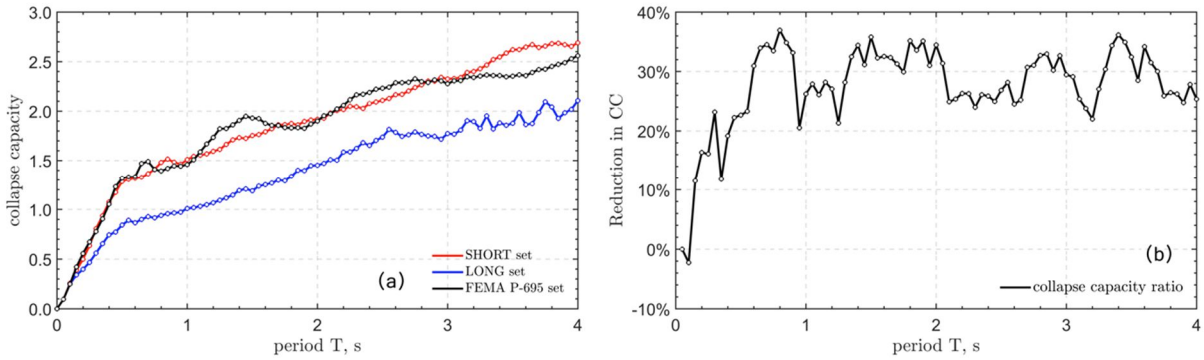

Figure 19. Median collapse capacity spectra for short duration, long duration and FEMA P-695 sets (a); Reduction in median CC estimated by the long duration set CCS, with respect to the short duration set (b).

6.2. Refined CCS and influence of key parameters

To explore further the relationship between ground motion duration, structural response at collapse and key structural properties, the full set of multi-storey frames introduced in Section 1 (Table 4) is considered herein through equivalent single-degree-of-freedom (ESDOF) structural models. The ESDOF systems were calibrated using the cyclic structural response of the multi-degree-of-freedom models, following the procedure described in Section 5.1 above. The 50 ESDOF models were subjected to IDA in order to determine the collapse capacity (i.e. Equation 3) due to the seismic action produced by both short and long ground motion duration sets. In addition, as before, the records in FEMA P-695 were considered to provide further insight and comparison with current seismic design procedures. Since hysteretic models better capture the influence of earthquake duration, especially at the collapse level (i.e., large nonlinear displacements), as considered in the previous section, degrading systems with calibrated equivalent rate of cyclic deterioration were used throughout. The results are presented in a manner resembling the collapse capacity spectra (CCS), since the structural systems considered represent a wide range of fundamental periods (T_1) of vibration. As the spectral range is defined through information from the actual structures, it is henceforth referred to as *refined collapse capacity spectra.* In addition, the computed collapse capacity for the different systems are analysed with respect to the structural properties of interest, including the *global lateral stiffness* (τ) and the *equivalent rate of cyclic degradation* (Λ). The influence of key parameters on CCS, namely the fundamental period, lateral stiffness, and deterioration rate, is examined below.

6.2.1. Fundamental period

The collapse capacity is firstly assessed with respect to the fundamental period of vibration for the whole family of structures considered. Figure 20 (a) and (b) show the refined collapse capacity spectra for short ($\mathrm{CC}_{\mathrm{short}}$) and long ($\mathrm{CC}_{\mathrm{long}}$) ground motion duration sets, respectively. As observed before, the collapse capacity shows a clear trend with respect to the fundamental period, regardless of the ground motion set. In addition, by direct comparison of the results in (a) and (b), the reduction in collapse capacity is evident throughout. A direct comparison between $\mathrm{CC}_{\mathrm{short}}$ and $\mathrm{CC}_{\mathrm{long}}$ is presented in Figure 20 (d) as a reduction in median collapse capacity, for each individual structural system. The arithmetic mean of the collapse capacity reduction due to ground motion duration is about 20%, and a moderate trend with respect to the fundamental period can be observed, exhibiting a more significant reduction in CC as T_1 increases. Additionally, and as a benchmark, Figure 20 (c) shows the computed refined collapse capacity spectrum for to the FEMA P-695 ($\mathrm{CC}_{\mathrm{FEMA}}$) duration-blind ground motion record set. As seen before (e.g. Figure 19 (a)), the $\mathrm{CC}_{\mathrm{FEMA}}$ quantities are in close agreement with the short duration set. A building-by-building comparison is not provided here for brevity, but an average of about a 6% higher CC is obtained for the FEMA set of records compared to the short set. Therefore, when FEMA P-695 blind-duration ground motion records set is utilised, the collapse capacity outcome tends to be closer to that obtained by a short duration set of records, albeit on the non-conservative side.

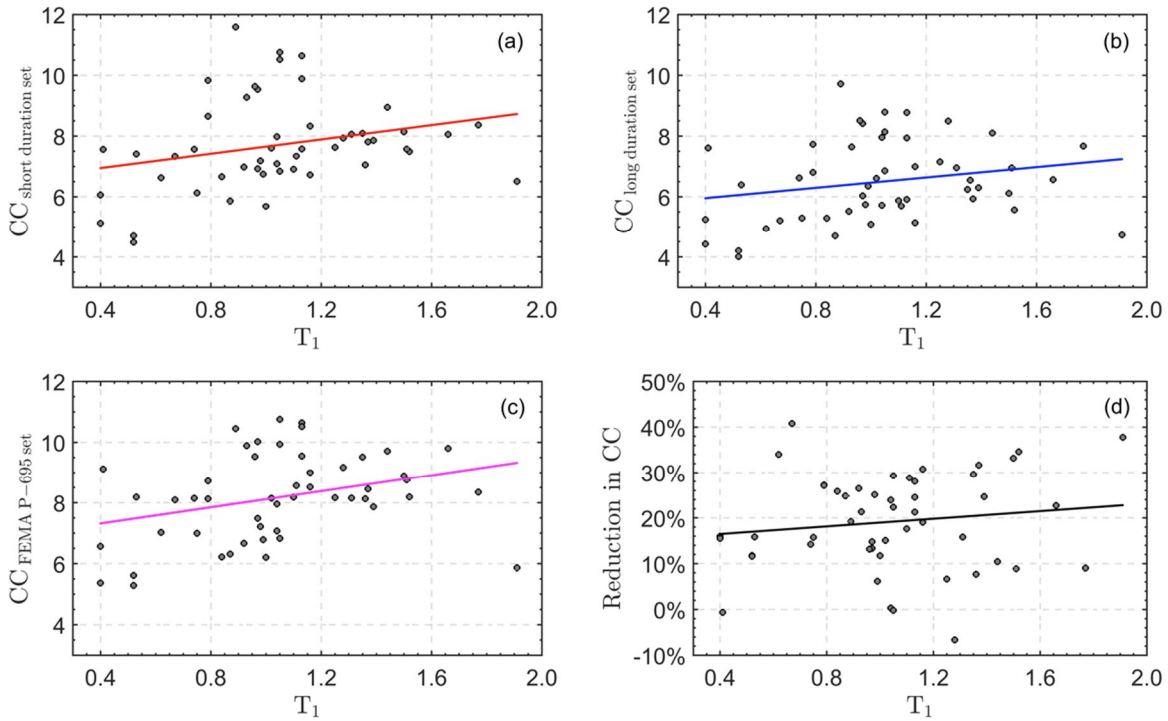

Figure 20. Collapse capacity spectra due to short (a) and long (b) duration set, besides FEMA P-695 set (c). Ratio between short and long duration set represented by a decrease in collapse capacity (d).

6.2.2. Global lateral stiffness

The global normalized stiffness of a steel frame, τ, determined as the ratio between the fundamental period of vibration (T_1), and the number of stories (N), is also considered to assess the influence of ground motion duration on the collapse performance. As presented in Table 4, the global stiffness values range from about 0.1 to 0.3, in agreement with values typically obtained in steel moment frames. Figure 21 (a) and (b) present the median collapse capacity versus global stiffness for short and long duration sets, respectively. In general, an opposite trend is observed compared to the fundamental period, as in this case the collapse capacity decreases as the lateral stiffness increases. The influence of duration is directly determined in Figure 21 (d) through the percentage reduction in CC. As shown in the figure, a higher influence from ground motion duration is obtained as the lateral stiffness increases. The collapse capacities due to the reference records set corresponding to FEMA P-695 shown in Figure 21 (c) presents a slightly different behavior, where an observable increase in the CC occurs as the lateral stiffness increases.

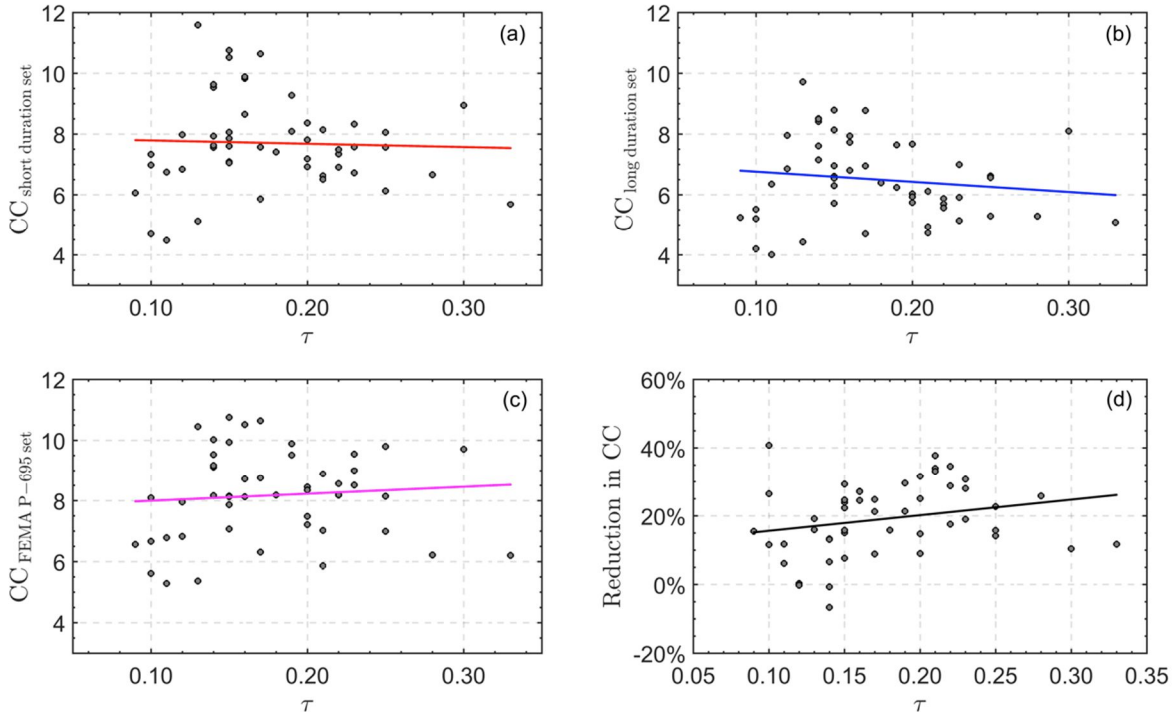

Figure 21. Collapse capacity as function of lateral stiffness (τ) due to short (a) and long (b) duration set, besides FEMA P-695 set (c). Reduction in CC between short and long duration sets (d).

6.2.3. Cyclic deterioration rate

Based on the initial results described in Section 5 above regarding the influence of cyclic deterioration rate Λ on the structural collapse performance, this subsection includes an extended analysis on the influence of Λ for the whole set of equivalent systems and the different record sets. In addition, the cyclic deterioration rates are perturbed by pushing each individual central value above and below the equivalent Λ for the reference frames while maintaining the values of all other parameters. The sensitivity of Λ is then evaluated by performing additional incremental dynamic analyses in order to compute the median collapse capacity for all the structural systems and respective ground motion record sets. Before discussing the results in detail, a number of observations are firstly worth noting. The equivalent cyclic rate of deterioration of a structural system depends on several structural parameters, such as the fundamental period of vibration, lateral stiffness and mass participation ratio. Therefore, the following procedure, where each structural system is modelled considering the calibrated equivalent rate of cyclic deterioration, may offer further insight, added to those made above in Section 6.1 on the influence of duration.

The relationship between the median collapse capacity and equivalent Λ for the reference frames is shown in Figure 22. As expected, a clear trend is observed between CC and the equivalent Λ, where CC increases with higher Λ; i.e. when the rate of cyclic deterioration is lower. Subfigures (a) and (b) show CC values due to short and long ground motion duration sets, respectively. When directly compared in order to determine the reduction in collapse capacity through different levels of equivalent Λ due to duration, a clear trend is observed as indicated in Figure 22 (d). For the fastest rates of cyclic degradation, up to 40% of collapse capacity reduction is observed due to duration, whilst for the slowest rates of cyclic degradation, the influence becomes insignificant.

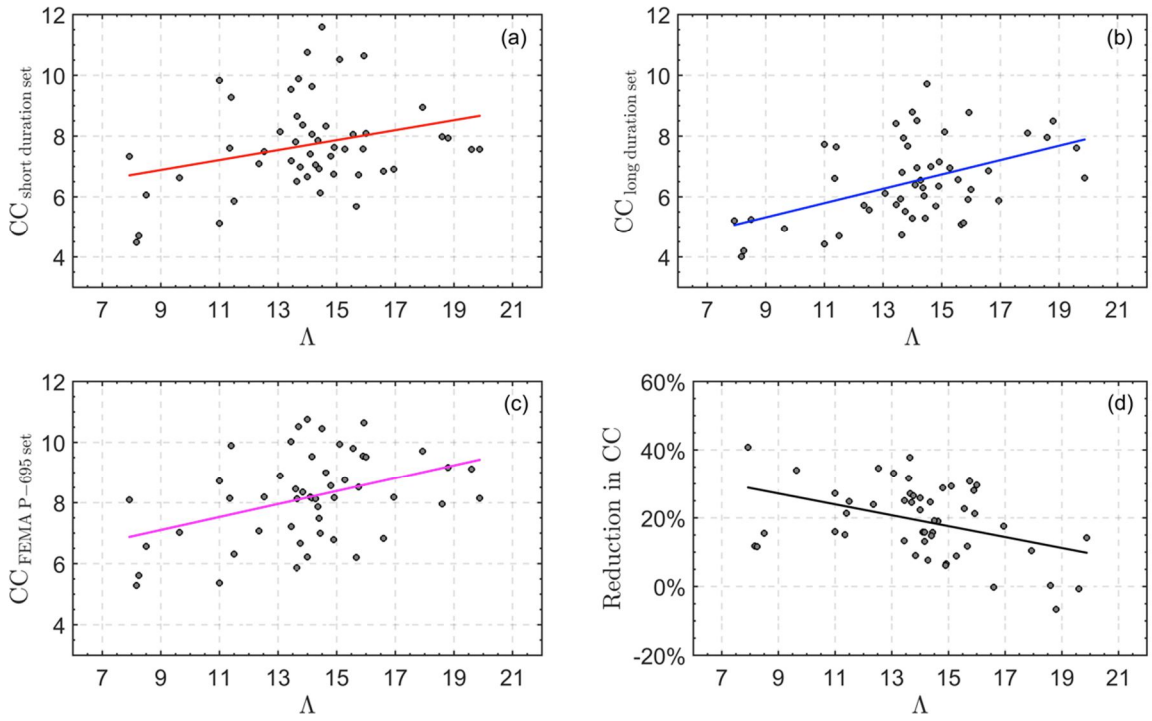

Figure 22. Collapse capacity as a function of equivalent cyclic rate of degradation (Λ) due to short (a) and long (b) duration sets, besides the FEMA P-695 set (c). Reduction in CC between short and long duration sets (d).

By perturbing the equivalent rate of cyclic deterioration, for all the structural systems by equal percentages, towards faster and slower rates, further IDA were performed to quantify median collapse capacities. The equivalent Λ for the reference frames is represented herein as '100% of Λ'. The faster perturbed cyclic rate of degradation corresponds to a 25% reduction of Λ and is henceforth referred to as '75% of Λ'. Similarly, the slower perturbed cyclic rate of degradation considers a 25% increase in Λ and is therefore designated as '125% of Λ'. Those absolute levels of disturbance of Λ from the reference frames are considered to be reasonable values based on the observed distribution of Λ for structural systems with similar fundamental periods and similar levels of lateral stiffness.

The results for the three levels of cyclic degradation rates are presented in Figure 23. As before, short and long ground motion duration sets are considered, besides the FEMA P-695 set, as in subfigures (a), (b) and (c), respectively. Using the same format as before, the refined CCS results are presented with respect to T_1. For the case of spectrally equivalent short duration records, shown in Figure 23 (a), the most noticeable observation is the insignificant change in CC between the trend lines of the three systems throughout the period range. This indicates that when subjected only to short duration records, the rate of cyclic deterioration does not play a significant role in the estimation of median CC irrespective of the fundamental period of the structure. On the other hand, for the case of spectrally equivalent long duration records, shown in Figure 23 (b), a moderate disturbance in Λ may instigate notable differences in the median collapse capacity. Across the spectral region, the effect of a decrease or increase of Λ shows a largely steady behaviour. When the equivalent cyclic rate of degradation is increased (i.e. 75% of Λ), a 12% constant decrease in the median collapse capacity is obtained with respect to the reference frames. When the cyclic rate of degradation is reduced, a moderate 5% constant increase in the median collapse capacity is observed compared to the reference frames (i.e. 100% of Λ). Lastly, the case of the duration-blind ground motion records of FEMA-P-695, shown in Figure 23 (c), indicate virtually no difference between the three cyclic degradation rates, which is broadly similar to the short duration case.

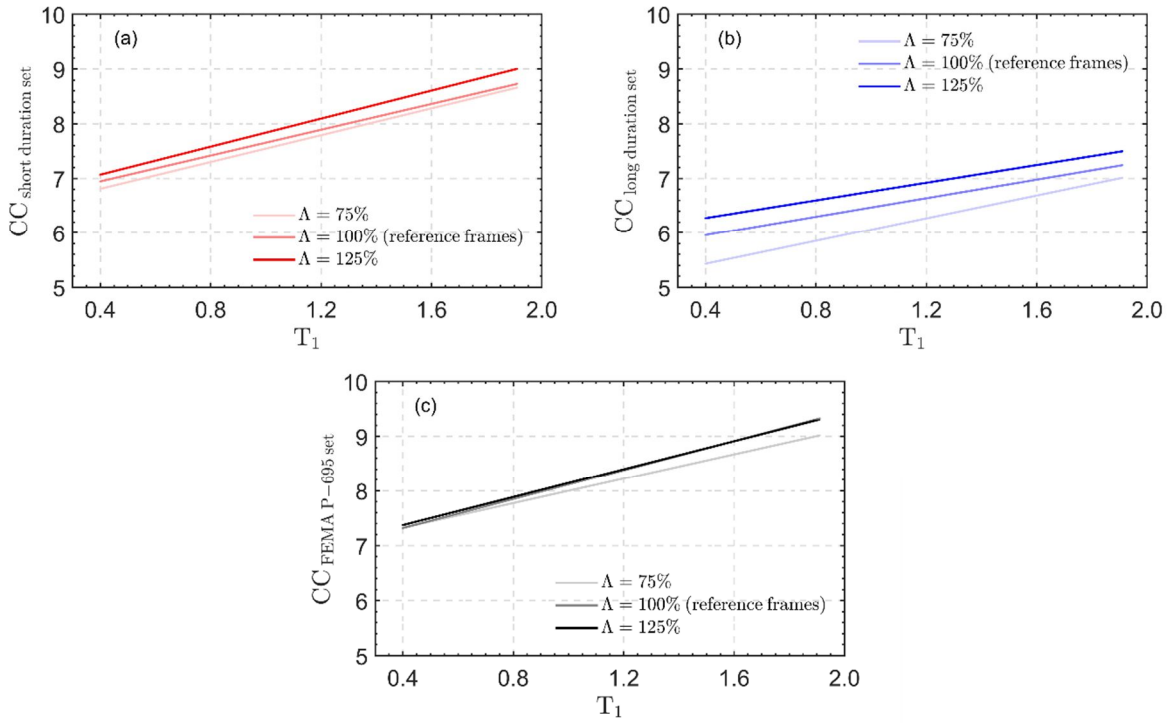

Figure 23. Refined collapse capacity spectra as a function of T_1 for perturbed rates of cyclic deterioration: (a) short duration set, (b) long duration set, and (c) FEMA P-695 set.

Finally, as the main objective of this study is to gain further insight on the influence of earthquake duration, a direct comparison between the CC results obtained for the case of short and long duration sets are presented in Figure 24, considering the corresponding levels of cyclic deterioration. As above, the results are presented as a percentage reduction in the median collapse capacity, for each individual level of Λ. Besides, the variation in median CC is arranged with respect to the fundamental period, T_1, global lateral stiffness, τ, and the equivalent Λ for the reference frames. The first general observation from the figure is that, on average, there is a more significant difference in the median CC between the reference frames and the increased rate of cyclic degradation. This is consistent with the sensitivity analysis carried out in Section 5 above, where an exponential reduction in the median CC is observed as Λ decreases, in contrast to a relatively moderate change in the median CC as Λ increases, reaching a saturation level.

Presenting the results with respect to the fundamental period of vibration, as shown in Figure 24 (a), a higher influence of Λ on the reduction in median CC due to duration can be observed for relatively low values of T_1. On the other hand, a constant decrease of 23% is observed in the median CC due to duration irrespective of the rate of cyclic degradation for systems with higher fundamental periods of vibration. When presented with respect to the global lateral stiffness, a constant trend in the reduction of median CC is observed, as shown in Figure 24 (b), regardless of the level of lateral stiffness. Up to 30% reduction in median CC for flexible (i.e. higher τ) systems due to the increased rate of Λ. Lastly, the results are arranged by the cyclic degradation rate, belonging to the reference frames (i.e. 100% of Λ), as shown in Figure 24 (c). When lower values of equivalent Λ are disturbed, higher difference in the median CC are obtained between the reference frames and the reduced case (i.e. 75% of Λ). A peak of 32% in the reduction in median collapse capacity due to duration is obtained for the fastest rate of cyclic degradation. When higher levels of equivalent Λ are used, no differences are noticeable between the reference frames and the reduced cyclic rate, in contrast with about 10% difference due to the increased Λ with respect to the reference frames.

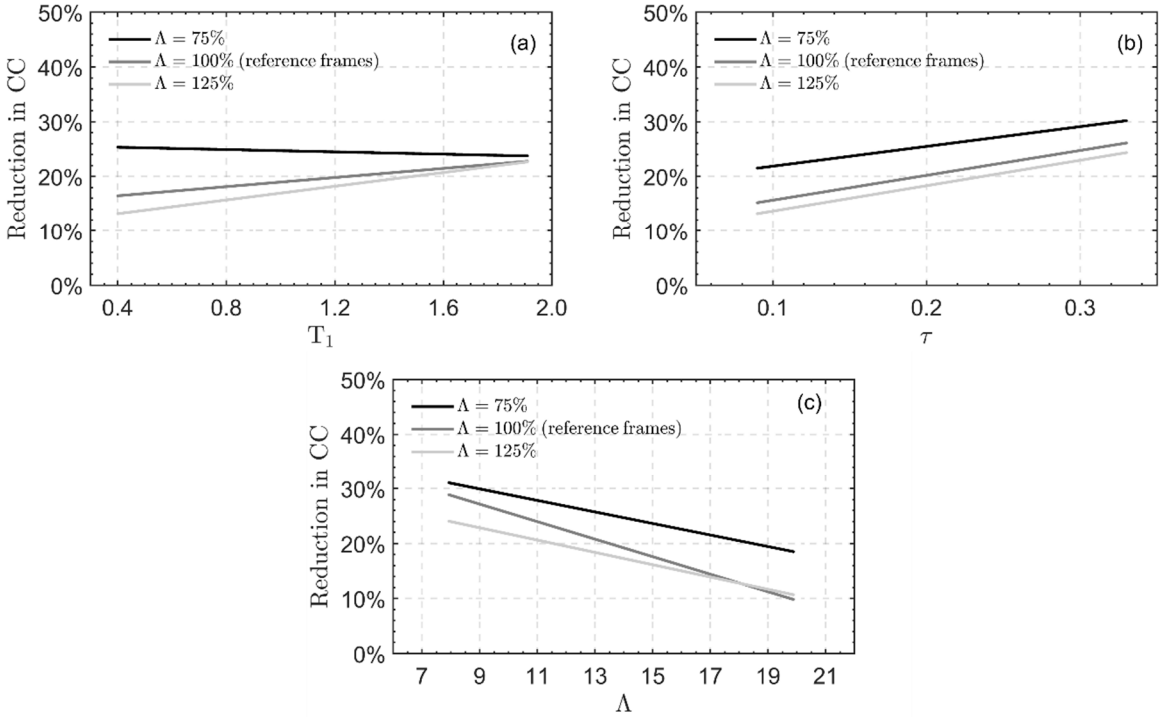

Figure 24. Reduction in median CC and Λ sensitivity due to duration between short and long duration sets, as a function of :(a) fundamental period, T_1; (b) lateral stiffness, τ; and (c) equivalent cyclic rate of deterioration, Λ.

7. CONCLUSIONS

This paper examined the influence of ground motion duration using an extensive suite of steel moment frames, with due account for in-cycle and cyclic degradation effects. A set of 77 spectrally equivalent pairs of short and long records (i.e., 144 individual records) was employed in the investigation in order to isolate the effect of ground motion duration within detailed nonlinear dynamic analysis. Several structural modelling levels varying from simplified single-degree-of-freedom representations to detailed models of selected multi-storey frames were adopted in the study. The results provided a detailed insight into the influence of earthquake duration at typical design levels of lateral strength demand. Collapse capacity spectra (CCS) were also employed to assess the influence of earthquake duration on structural collapse levels with respect to the fundamental period of vibration (T_1), global lateral stiffness (τ) and cyclic rate of degradation (Λ). Based on the findings, the main conclusions are summarised below.

In order to capture the influence of ground motion duration, particularly at ultimate levels of structural performance, it is essential to employ numerical models that are capable of representing in-cycle and cyclic degradation (in-cycle and cyclic) phenomena as well as P-delta effects. This study has also shown that such models may also be necessary for lower and typical design levels of seismic lateral strength demand, as widely-used non-degrading idealised representations are unable to reflect important duration-dependant behaviour.

The sensitivity analysis performed in this paper using a refined equivalent single-degree-of-freedom representation (ESDOF) of the multi-storey frames showed that the yield capacity of the system (M_y) and the post-yield stiffness ratio (α_h) play a notable role in the obtained structural collapse capacity. The influence of duration was also shown to be significant for lower stages of seismic performance, typically associated with design, particularly when relatively high rates of cyclic degradation levels (i.e., lower values of Λ) were used. Although the uncertainties associated with record-to-record variability were not explicitly quantified in this study, variation in post-yield stiffness had a clear influence on the structural behaviour at design levels of seismic performance due to the action of long duration earthquakes.

The influence of duration was shown to be particularly evident near collapse or dynamic instability. Incremental dynamic analysis on four selected multi-storey frames indicated a higher probability of

collapse for long duration ground motion records, with an average reduction of 17% in the median collapse capacity, with a maximum of 24%. When the study was extended to a broader range of idealised fundamental periods by examining collapse capacity spectra (CCS), reductions of up to 40% in the collapse capacity were observed, highlighting the inadequacy of typical seismic code procedures, which are largely based on short duration records. This was particularly evident when CCS was compared with results from a duration-independent set of records recommended by FEMA-P695.

The influence of the fundamental period, global lateral stiffness, and cyclic rate of degradation was considered with respect to earthquake duration, through the production of *refined collapse capacity spectra* based on the seismic performance of 50 steel moment frames. Median reductions of about 20% on the collapse capacity were observed due to duration. A higher influence from ground motion duration on collapse capacity was obtained for longer fundamental periods and higher levels of global lateral stiffness. Moreover, up to 40% reduction in the collapse capacity was obtained for the fastest rate of cyclic degradation corresponding relatively low but realistic practical values of cyclic deterioration. Overall, this study emphasises the importance of considering the influence of ground motion duration in seismic assessment and design procedures, and highlights the importance of accounting for degradation effects in order to capture key response characteristics that are otherwise typically disregarded.

This study shows that the new generation of performance-based guidelines can be significantly improved through the explicit inclusion of long duration records such as in the global set employed in this study. Similarly, in conventional seismic codes, where the analysis is typically based on modal analysis or a simplified lateral force method based on a target demand spectrum, simple modification factors for the forces and target spectra can be incorporated in order to account for the influence of duration effects.

ACKNOWLEDGMENTS

The first author would like to express his sincere gratitude to the “Consejo Nacional de Ciencia y Tecnología” (CONICYT, Chile) for the funding of his doctoral studies at Imperial College London.

NOTATION

T_1	:	Fundamental period of vibration
N_s	:	Number of stories
H	:	Total building height
τ	:	Global lateral stiffness
Λ	:	Cyclic rate of degradation
Γ	:	Modal participation factor
V_1	:	Base shear from capacity curve
M	:	Total seismic mass
C_R	:	Inelastic displacement ratio
S_d	:	Displacement of a linear equivalent system
R	:	Lateral strength ratio or strength reduction factor
SF	:	Scaling factor
M_y	:	Yield moment
α_h	:	Post-yield hardening slope
θ_p	:	Capping rotation
α_{pc}	:	Post-capping softening (negative slope)
r	:	Residual moment plateau
θ_u	:	Ultimate rotation
Δ	:	Inter-storey drift, rad
CC	:	Collapse capacity
CCS	:	Collapse capacity spectra
$S_a(T_1)$	:	Spectral acceleration at fundamental period
γ	:	Base shear coefficient of the system

REFERENCES

Adam, C. and Jäger, C., 2012. Dynamic instabilities of simple inelastic structures subjected to earthquake excitation. In: H. Irschik, M. Krommer and A. Belyaev (Editors), Advanced Dynamics and Model-Based Control of Structures and Machines. Springer, Vienna, pp. 11-18.

Ancheta, T.D., Darragh, R.B., Stewart, J.P., Seyhan, E., Silva, W.J., Chiou, B.S.-J., Wooddell, K.E., Graves, R.W., Kottke, A.R. and Boore, D.M., 2014. NGA-West2 database. Earthquake Spectra, 30(3): 989-1005.

ATC, 2010. ATC 72-1. Interim guidelines on modeling and acceptance criteria for seismic design and analysis of tall buildings, Redwood City, California., PEER/ATC.

Barbosa, A.R., Ribeiro, F.L. and Neves, L.A., 2017. Influence of earthquake ground-motion duration on damage estimation: application to steel moment resisting frames. Earthquake Engineering & Structural Dynamics, 46(1): 27-49.

Bhattacharya, S., Hyodo, M., Goda, K., Tazoh, T. and Taylor, C., 2011. Liquefaction of soil in the Tokyo Bay area from the 2011 Tohoku (Japan) earthquake. Soil Dynamics and Earthquake Engineering, 31(11): 1618-1628.

Bommer, J.J., Magenes, G., Hancock, J. and Penazzo, P., 2004. The influence of strong-motion duration on the seismic response of masonry structures. Bulletin of Earthquake Engineering, 2(1): 1-26.

Bommer, J.J. and Martinez-Pereira, A., 1999. The effective duration of earthquake strong motion. Journal of earthquake engineering, 3(02): 127-172.

Boore, D.M. and Bommer, J.J., 2005. Processing of strong-motion accelerograms: needs, options and consequences. Soil Dynamics and Earthquake Engineering, 25(2): 93-115.

Bravo-Haro, M.A., Tsitos, A. and Elghazouli, A.Y., 2018. Drift and rotation demands in steel frames incorporating degradation effects. Bulletin of Earthquake Engineering, 16(10): 4919-4950.

CEN, 2004a. EN-1998-1:2004 - Eurocode 8: Design of Structures for Earthquake Resistance – Part 1: General rules, seismic actions and rules for buildings. European Committee for Standardization, Brussels.

CEN, 2005. EN 1993-1-1: Eurocode 3: Design of Steel Structures. Part 1-1: General Rules and Rules for Buildings. Comité Europeo de Normalización.

Chandramohan, R., Baker, J.W. and Deierlein, G.G., 2016. Quantifying the influence of ground motion duration on structural collapse capacity using spectrally equivalent records. Earthquake Spectra, 32(2): 927-950.

Cornell, C.A., 1997. Does duration really matter? Proceedings of the FHWA/NCEER Workshop on the National Representation of Seismic Ground Motion for New and Existing Highway Facilities, Burlingame, California. Organized by NCEER project 106-F-5.4.1 and ATC project ATC-18-1.

De Luca, F., Vamvatsikos, D. and Iervolino, I., 2013. Near-optimal piecewise linear fits of static pushover capacity curves for equivalent SDOF analysis. Earthquake Engineering & Structural Dynamics, 42(4): 523-543.

Dutta, A. and Mander, J., 2001. Energy based methodology for ductile design of concrete columns. Journal of Structural Engineering, 127(12): 1374-1381.

FEMA, P., 695 (2009) Quantification of seismic performance factors. FEMA P-695 report, the Applied Technology Council for the Federal Emergency Management Agency, Washington, DC.

Foschaar, J., Baker, J. and Deierlein, G., 2012. Preliminary assessment of ground motion duration effects on structural collapse, Proceedings of the 15th world conference on earthquake engineering.

Gupta, A. and Krawinkler, H., 1999. Seismic demands for the performance evaluation of steel moment resisting frame structures, Stanford University.

Gupta, A. and Krawinkler, H., 2000. Dynamic P-delta effects for flexible inelastic steel structures. Journal of Structural Engineering, 126(1): 145-154.

Hancock, J. and Bommer, J.J., 2006. A state-of-knowledge review of the influence of strong-motion duration on structural damage. Earthquake spectra, 22(3): 827-845.

Hancock, J. and Bommer, J.J., 2007. Using spectral matched records to explore the influence of strong-motion duration on inelastic structural response. Soil Dynamics and Earthquake Engineering, 27(4): 291-299.

Ibarra, L.F., Medina, R.A. and Krawinkler, H., 2005. Hysteretic models that incorporate strength and

stiffness deterioration. Earthquake engineering & structural dynamics, 34(12): 1489-1511.
Iervolino, I., Manfredi, G. and Cosenza, E., 2006. Ground motion duration effects on nonlinear seismic response. Earthquake engineering & structural dynamics, 35(1): 21-38.
Lignos, D.G. and Krawinkler, H., 2007. A database in support of modeling of component deterioration for collapse prediction of steel frame structures, Structural Engineering Research Frontiers, pp. 1-12.
Lignos, D.G. and Krawinkler, H., 2010. Deterioration modeling of steel components in support of collapse prediction of steel moment frames under earthquake loading. Journal of Structural Engineering, 137(11): 1291-1302.
McKenna, F., 2011. OpenSees: a framework for earthquake engineering simulation. Computing in Science & Engineering, 13(4): 58-66.
Ou, Y.-C., Song, J., Wang, P.-H., Adidharma, L., Chang, K.-C. and Lee, G.C., 2013. Ground motion duration effects on hysteretic behavior of reinforced concrete bridge columns. Journal of Structural Engineering, 140(3): 04013065.
Raghunandan, M. and Liel, A.B., 2013. Effect of ground motion duration on earthquake-induced structural collapse. Structural Safety, 41: 119-133.
Rahnama, M. and Krawinkler, H., 1993. Effect of soft soils and hysteresis models on seismic design spectra. Rep. No. TB, 108.
Rathje, E.M., Abrahamson, N.A. and Bray, J.D., 1998. Simplified frequency content estimates of earthquake ground motions. Journal of Geotechnical and Geoenvironmental Engineering, 124(2): 150-159.
Saragoni, R.G. and Hart, G.C., 1973. Simulation of artificial earthquakes. Earthquake Engineering & Structural Dynamics, 2(3): 249-267.
Sarieddine, M. and Lin, L., 2013. Investigation correlations between strong-motion duration and structural damage. In: B. Leshko and J. McHugh (Editors), Structures Congress 2013: Bridging Your Passion with Your Profession, pp. 2926-2936.
Tremblay, R., 1998. Development of design spectra for long-duration ground motions from Cascadia subduction earthquakes. Canadian Journal of Civil Engineering, 25(6): 1078-1090.
Trifunac, M.D. and Brady, A.G., 1975. A study on the duration of strong earthquake ground motion. Bulletin of the Seismological Society of America, 65(3): 581-626.
Tsitos, A., Bravo-Haro, M.A. and Elghazouli, A.Y., 2018. Influence of deterioration modelling on the seismic response of steel moment frames designed to Eurocode 8. Earthquake Engineering & Structural Dynamics, 47(2): 356-376.
Vamvatsikos, D. and Cornell, C.A., 2002. Incremental dynamic analysis. Earthquake Engineering & Structural Dynamics, 31(3): 491-514.
Verdugo, R. and González, J., 2015. Liquefaction-induced ground damages during the 2010 Chile earthquake. Soil Dynamics and Earthquake Engineering, 79: 280-295.
Xie, L.-L. and Zhang, X., 1988. Engineering duration of strong motion and its effects on seismic damage, Proceedings of the Ninth World Conference on Earthquake Engineering, pp. 307-12.